# Five new pseudocryptic land planarian species of *Cratera* (Platyhelminthes: Tricladida) unveiled through integrative taxonomy (#48478)

First submission

## Guidance from your Editor

Please submit by **5 Jun 2020** for the benefit of the authors  (and your $200 publishing discount) .

### Structure and Criteria
Please read the 'Structure and Criteria' page for general guidance.

### Custom checks
Make sure you include the custom checks shown below, in your review.

### Author notes
Have you read the author notes on the guidance page?

### Raw data check
Review the raw data.

### Image check
Check that figures and images have not been inappropriately manipulated.

Privacy reminder: If uploading an annotated PDF, remove identifiable information to remain anonymous.

## Files
Download and review all files from the materials page.

17 Figure file(s)
2 Table file(s)

## Custom checks

**DNA data checks**

- Have you checked the authors data deposition statement?
- Can you access the deposited data?
- Has the data been deposited correctly?
- Is the deposition information noted in the manuscript?

**Field study**

- Have you checked the authors field study permits?
- Are the field study permits appropriate?

**New species checks**

- Have you checked our new species policies?

Do you agree that it is a new species?

Is it correctly described e.g. meets ICZN standard?

For assistance email [peer.review@peerj.com](mailto:peer.review@peerj.com)

## Structure your review

The review form is divided into 5 sections. Please consider these when composing your review:

1. **BASIC REPORTING**
2. **EXPERIMENTAL DESIGN**
3. **VALIDITY OF THE FINDINGS**
4. General comments
5. Confidential notes to the editor

📄 You can also annotate this PDF and upload it as part of your review

When ready [submit online](#).

## Editorial Criteria

Use these criteria points to structure your review. The full detailed editorial criteria is on your [guidance page](#).

### BASIC REPORTING

✓ Clear, unambiguous, professional English language used throughout.

✓ Intro & background to show context. Literature well referenced & relevant.

✓ Structure conforms to [PeerJ standards](#), discipline norm, or improved for clarity.

✓ Figures are relevant, high quality, well labelled & described.

✓ Raw data supplied (see [PeerJ policy](#)).

### EXPERIMENTAL DESIGN

✓ Original primary research within [Scope of the journal](#).

✓ Research question well defined, relevant & meaningful. It is stated how the research fills an identified knowledge gap.

✓ Rigorous investigation performed to a high technical & ethical standard.

✓ Methods described with sufficient detail & information to replicate.

### VALIDITY OF THE FINDINGS

ⓘ Impact and novelty not assessed. Negative/inconclusive results accepted. *Meaningful* replication encouraged where rationale & benefit to literature is clearly stated.

✓ All underlying data have been provided; they are robust, statistically sound, & controlled.

✓ Speculation is welcome, but should be identified as such.

✓ Conclusions are well stated, linked to original research question & limited to supporting results.

# Standout reviewing tips

The best reviewers use these techniques

| Tip | Example |
| --- | --- |
| **Support criticisms with evidence from the text or from other sources** | *Smith et al (J of Methodology, 2005, V3, pp 123) have shown that the analysis you use in Lines 241-250 is not the most appropriate for this situation. Please explain why you used this method.* |
| **Give specific suggestions on how to improve the manuscript** | *Your introduction needs more detail. I suggest that you improve the description at lines 57- 86 to provide more justification for your study (specifically, you should expand upon the knowledge gap being filled).* |
| **Comment on language and grammar issues** | *The English language should be improved to ensure that an international audience can clearly understand your text. Some examples where the language could be improved include lines 23, 77, 121, 128 – the current phrasing makes comprehension difficult.* |
| **Organize by importance of the issues, and number your points** | *1. Your most important issue*<br>*2. The next most important item*<br>*3. …*<br>*4. The least important points* |
| **Please provide constructive criticism, and avoid personal opinions** | *I thank you for providing the raw data, however your supplemental files need more descriptive metadata identifiers to be useful to future readers. Although your results are compelling, the data analysis should be improved in the following ways: AA, BB, CC* |
| **Comment on strengths (as well as weaknesses) of the manuscript** | *I commend the authors for their extensive data set, compiled over many years of detailed fieldwork. In addition, the manuscript is clearly written in professional, unambiguous language. If there is a weakness, it is in the statistical analysis (as I have noted above) which should be improved upon before Acceptance.* |

# Five new pseudocryptic land planarian species of *Cratera* (Platyhelminthes: Tricladida) unveiled through integrative taxonomy

**Ana Paula G Araujo** [1, 2] , **Fernando Carbayo** [2, 3] , **Marta Riutort** [4] , **Marta Álvarez-Presas** [Corresp. 4]

[1] Museu de Zoologia, Universidade de São Paulo, São Paulo, Brazil

[2] Laboratório de Ecologia e Evolução, Escola de Artes, Ciências e Humanidades, Universidade de São Paulo, São Paulo, Brazil

[3] Departamento de Zoologia, Instituto de Biociências, Universidade de São Paulo, São Paulo, Brazil

[4] Departament de Genètica, Microbiologia i Estadística, Facultat de Biologia and Institut de Recerca de la Biodiversitat (IRBio), Universitat de Barcelona, Barcelona, Spain

Corresponding Author: Marta Álvarez-Presas
Email address: onaalvarez@ub.edu

**Background.** *Cratera* is a genus of land planarians endemic to the Atlantic forest. The species of this genus are distinguished from each other by a series of external and internal characters, nonetheless they represent a challenging taxonomic issue due to the extreme alikeness of the species analysed on the present work. To resolve these difficulties, we have performed morphological analyses and used five nuclear and mitochondrial genes in an integrative taxonomic study.

**Methods**. To unveil eventual cryptic species, we applied a molecular species delimitation approach based on molecular discovery methods, followed by a validation method. The putative species so delimited were then validated on the basis of the existence of morphological features that differentiated them.

**Results**. By doing so, we have discovered and described four new species, namely *Cratera piguaiassu, C. piguaiatui, C. piguaiaboja,* and *C. imbiri*. A fifth new species, *C. paraitinga* was not highly supported by molecular evidence but was described because its morphological attributes were unique. As a result, we find again the existence of high similarity among terrestrial planarians as has already been described in other genera. The high number of young species poorly differentiated might be explained by the recent history of the area.

1 # Five new pseudocryptic land planarian species of
2 # *Cratera* (Platyhelminthes: Tricladida) unveiled through
3 # integrative taxonomy
4
5

6 Ana Paula G. Araujo[1,3], Fernando Carbayo[2,3], Marta Riutort[4], Marta Álvarez-Presas[4]
7
8 [1] Museu de Zoologia da Universidade de São Paulo, Ipiranga, São Paulo, SP, Brazil
9 [2] Departamento de Zoologia, Instituto de Biociências, Universidade de São Paulo, São Paulo, SP,
10 Brazil
11 [3] Laboratório de Ecologia e Evolução, Escola de Artes, Ciências e Humanidades, Universidade
12 de São Paulo, São Paulo, SP, Brazil
13 [4] Departament de Genètica, Microbiologia i Estadística, Facultat de Biologia and Institut de
14 Recerca de la Biodiversitat (IRBio), Universitat de Barcelona, Barcelona, Catalonia, Spain
15
16 Corresponding Author:
17 Marta Álvarez-Presas[4]
18 Av. Diagonal 645, Barcelona, Catalonia, 08028, Spain
19 Email address: coseseries@gmail.com
20

21 ## Abstract

22 **Background.** *Cratera* is a genus of land planarians endemic to the Atlantic forest. The species of

23 this genus are distinguished from each other by a series of external and internal characters,

24 nonetheless they represent a challenging taxonomic issue due to the extreme alikeness of the

25 species analysed on the present work. To resolve these difficulties, we have performed

26 morphological analyses and used five nuclear and mitochondrial genes in an integrative

27 taxonomic study.

28 **Methods**. To unveil eventual cryptic species, we applied a molecular species delimitation

29 approach based on molecular discovery methods, followed by a validation method. The putative

30 species so delimited were then validated on the basis of the existence of morphological features

31 that differentiated them.

32 **Results**. By doing so, we have discovered and described four new species, namely *Cratera*

33 *piguaiassu, C. piguaiatui, C. piguaiaboja,* and *C. imbiri*. A fifth new species, *C. paraitinga* was

34    not highly supported by molecular evidence but was described because its morphological

35    attributes were unique. As a result, we find again the existence of high similarity among

36    terrestrial planarians as has already been described in other genera. The high number of young

37    species poorly differentiated might be explained by the recent history of the area.

38

## Introduction

40        Land planarians (Platyhelminthes: Tricladida: Geoplanidae) are mostly soil inhabitants of

41    forested areas. There are over 900 known species (Sluys, 2016), 332 of them belonging to

42    Geoplaninae (http://planarias.each.usp.br; accessed in 18. March 2020), an exclusively

43    Neotropical subfamily. Anatomy and histology of the copulatory apparatus are central for the

44    identification and systematics of these organisms (e.g. E. M. Froehlich, 1955; Negrete & Brusa,

45    2016). Nonetheless, when traditional, morphology-based taxonomic approaches had been

46    complemented with molecular methodologies in different studies, some nominal species were

47    found to be polyphyletic (Sluys et al., 2016; Carbayo et al., 2018; Almeida, Marques & Carbayo,

48    2019). Reanalyses of the morphological evidence in those cases revealed that morphological

49    variation assumed to represent within species polymorphisms, turned out to signal distinct

50    species. From another perspective, reinterpretation of intra-specific morphological variation

51    revealed pseudocryptic species (see references above; Sáez & Lozano, 200█

52        The systematics of Geoplaninae above the species level has also benefited from the

53    molecular approach. Molecular phylogenetic analyses of this group revealed a number of

54    polyphyletic genera, one of them, *Geoplana* Stimpson, 1857 was subsequently split into several

55    genera (Carbayo et al., 2013). *Cratera* Carbayo et al., 2013 emerged from *Geoplana* as a

56    monophyletic group with 9 species to which were gradually added another 9 species with similar

57    features. The most conspicuous diagnostic feature of *Cratera* is an ejaculatory duct with its distal

58    section dilatated (Marcus, 1951; Lago-Barcia & Carbayo, 2018). However, this feature is not

59    found in all members of the genus, probably as a result of a secondary loss (Lago-Barcia &

60    Carbayo, 2018).

61        In the course of extensive land planarian samplings across the Atlantic forest we have

62    found many individuals that can be attributed to the *Cratera* genus, most of them presenting very

63    similar or even identical features in their external aspect or their internal anatomy. Given the

64    precedents of the existence of cryptic, or pseudocryptic species in other land planarian genera,

65    we set an integrative taxonomic analysis to unveil eventual cryptic species. We adopted the

66    General Lineage Species Concept, that defines species as independently evolving

67    metapopulation lineages (de Queiroz, 1998). To implement this concept, we have used an

68    integrative approach to species delimitations. We applied molecular species delimitation

69    methods to delineate a Primary Species Hypothesis (PSH) based on discovery methods, and

70    thereafter applied a validation method to formulate the Secondary Species Hypothesis (SSH;

71    Puillandre et al. 2012a). We then searched whether the putative species presented morphological

72    features giving support to their validity or not. By doing so we unveiled four species for which

73    molecular and morphological data are coherent with each other. Molecular data of a putative

74    fifth species did not fully support its distinctness, but morphological data did; in this case we

75    gave priority to the latter line of evidence to propose a new species.

76

77    **Materials & Methods**

78    **Specimens sampling and morphological study**

79        Intensive samplings were performed in four localities (75 hours sampling in Campos do

80    Jordão; 200 hours sampling in the remaining localities). Field experiments were approved by

81    COTEC - Instituto Florestal do Estado de São Paulo (Proc. SMA 12.640/2011), Museu de

82 Zoologia (EBBAut.020/2013) and Instituto Chico Mendes de Conservação da Biodiversidade

83 (Proc. 32779-1; 11748-4). Animals were collected from the soil litter during the day and at night.

84 The worms were photographed and, subsequently, killed in boiling water, after which a small

85 tissue sample was taken and preserved it in 100% ethanol for DNA extraction. Vouchers of

86 frozen tissues are kept in FC's laboratory. The remaining part of the body was fixed in 10%

87 formalin and, subsequently, transferred to 80% ethanol. Parts of the body were embedded in

88 paraffin Histosec®, sectioned at 2-7 µm, mounted on glass slides, and subsequently stained with

89 Mallory method as modified by Cason (1950). Slides were examined with a compound

90 microscope. Reconstruction drawings were done with a camera lucida attached to the

91 microscope. Photomicrographs were taken with the help of a digital camera attached to the

92 microscope. Enhancement of the contrast of the microphotographs and a whitish background of

93 the photomicrographs were done with GIMP (GNU Image Manipulation Program 2.8.16; The

94 GIMP team www.gimp.org, 1995-2016). Drawings and photomicrographs of sagittal and

95 horizontal views are orientated with anterior to the left. The width of the creeping sole was

96 measured on transverse sections of the pre-pharyngeal region. Type material was deposited in the

97 Museu de Zoologia da Universidade de São Paulo (MZUSP).

98      The electronic version of this article in Portable Document Format (PDF) will represent a

99 published work according to the International Commission on Zoological Nomenclature (ICZN),

100 and hence the new names contained in the electronic version are effectively published under that

101 Code from the electronic edition alone. This published work and the nomenclatural acts it

102 contains have been registered in ZooBank, the online registration system for the ICZN. The

103 ZooBank LSIDs (Life Science Identifiers) can be resolved and the associated information viewed

104 through any standard web browser by appending the LSID to the prefix http://zoobank.org/. The

105   LSID for this publication is: urn:lsid:zoobank.org:pub:F6B30CB7-6114-434F-9B2A-

106   A2F4CE625A20. The online version of this work is archived and available from the following

107   digital repositories: PeerJ, PubMed Central and CLOCKSS.

108

109   **Molecular data acquisition**

110         Extractions of genomic DNA were performed using the Wizard® Genomic DNA

111   Purification kit (Promega, Madison, WI, USA) following Álvarez-Presas et al. (2011). Two

112   mitochondrial and four nuclear markers were selected. The mitochondrial markers are a

113   cytochrome oxidase I gene fragment (hereafter referred to as COI), and a mitochondrial fragment

114   which includes the end of the nad4 gene, all the sequence of trnF and the beginning of the cox1

115   gene. This latter marker, hereafter referred to as Nd4toCox1, is tested for the first time in this

116   work. The four nuclear genes correspond to the 18S rDNA type II (18S), a fragment of the 28S

117   rDNA (28S), a partial coding region of the elongation factor 1-alpha gene (hereafter referred to

118   as EF), and an anonymous nuclear marker (hereafter referred as Tnuc813) developed from NGS

119   data (as exposed in Leria et al., 2019) and tested here for the first time. Primers used to amplify

120   and sequence the genes are available in Table S1. For some individuals (indicated in Table 1), it

121   was not possible to obtain a long COI sequence (~900 bp) of good quality (fragment amplified

122   by the BarS / COIR primers). To overcome this situation, a shorter fragment (COIF / COIR

123   primers), of ~300 bp, was amplified. The polymerase chain reaction (PCR) amplification (25 µL)

124   was performed on a Techne® TC-5000TM (Bibby Scientific Ltd, Staffordshire, UK) and on an

125   Eppendorf Mastercycler® (Eppendorf, Hamburg, Germany) personal thermocyclers using initial

126   denaturation step of 5 min at 92–95 °C, followed by 30–35 cycles of 30- to 50-s denaturation at

127   94–95 °C, 30- to 45-s annealing at 44–54 °C and 50-s – 1-min extension at 72 °C, with a final

128   extension step of 3–4 min at 72 °C. The PCR results were verified using electrophoresis of the

129   amplification products on 1% agarose gels stained with GelRed (Biotium, Hayward, CA, USA),

130   and visualized under UV transillumination. Amplification products were purified with a vacuum

131   manifold (Multiscreen®HTS Vacuum Manifold; Millipore Corporation, Billerica, MA, USA).

132   Purification products were sent to Macrogen (Amsterdam, Europe), were both strands where

133   sequenced by Sanger sequencing. Chromatograms were revised and contigs constructed in

134   Geneious v 8.1.7. software (Biomatters; available from http://www.geneious.com).

135        For all the coding genes (COI, Nd4toCox1, EF and Tnuc813), sequences were aligned

136   based on the amino acid sequences using Clustal W (included in the BioEdit software 7.0.9.0

137   (Hall, 1999)). The genetic code 9 (Echinoderm and flatworms' mitochondrial) was used for

138   translating the mitochondrial genes. Ribosomal RNA gene sequences were aligned using the

139   online version of the software Mafft v7 (Katoh, Rozewicki & Yamada, 2017) applying the G-

140   INS-i iterative refinement method. Misaligned or ambiguously aligned regions were removed

141   using Gblocks v0.91b program (Talavera & Castresana, 2007) allowing 50 as a maximum

142   number of contiguous non-conserved positions and setting the minimum length of a block to 4,

143   and half gap positions allowed. Three different datasets were used for several analyses: (1) *COI*

144   dataset including COI sequences used for the ABGD and mPTP molecular species delimitation

145   approaches; (2) *BPP* datasets 18S, 28S, COI, Nd4toCox1, Tnuc813, and EF independent

146   alignments (completing some sequences with missing data (Ns); see Table 1) used for the BPP

147   molecular species delimitation analysis; and (3) *concatenated* dataset, included the information

148   of the six genes (18S, 28S, EF, Tnuc813, COI and Nd4toCox1) and was used to infer a general

149   phylogeny.

150       For the individual gene alignments DNA sequence evolution model that better fits the

151    data was estimated by using jModelTest v2.1.4 (Darriba et al., 2012), applying the Akaike

152    information criterion (AIC). For the concatenated dataset PartitionFinder2 version 2.1.1 (Lanfear

153    et al., 2017) was run on the CIPRES Science Gateway (Miller, Pfeiffer & Schwartz, 2010) to

154    identify an appropriate partition scheme and their corresponding DNA evolutionary models. The

155    data were divided by gene, with unlinked branch lengths, the 'raxml' models for selection and the

156    AICc model selection criteria with the 'greedy' search algorithm. The phylogenetic trees for the

157    concatenated dataset were inferred using the Bayesian Inference (BI) method using MrBayes

158    software v3.2.6. (Ronquist et al., 2012) implemented in CIPRES and using BEAGLE (Ayres et

159    al., 2012), setting the evolutionary model and appropriate partitions according to the

160    PartitionFinder results with the unlinked parameters. Two runs of four chains were applied

161    producing 5 million generations and, for each of them, 5,000 trees were stored. It was checked

162    that the probability values (logarithm) of the cold chain reached the stationarity state and the

163    convergence of the two runs, verifying that the average standard deviation of the split

164    frequencies was lower than 0.01. A default burn-in of 25% was used and a consensus tree was

165    obtained from the remaining trees. The maximum likelihood (ML) method was used to infer

166    phylogenies with the software IQtree v1.6.10 (Nguyen et al., 2015). The IQtree searches were

167    carried out using the default configuration in CIPRES, with a starting random tree (option -t

168    RANDOM), and assessing branch support using 1000 ultrafast bootstrap approximation

169    replicates (Minh, Nguyen & Von Haeseler, 2013). The best fit models for each partition were the

170    selected by PartitionFinder and each partition was allowed to have its own set of branch lengths

171    (option -sp).

172

173  **Molecular species delimitation**

174     For the molecular species delimitation analyses, two discovery methods (ABGD and

175  mPTP) and one validation method (BPP) were applied. Using the COI dataset, the Automatic

176  Barcode Gap Discovery (ABGD) method (Puillandre et al., 2012b) was applied through the

177  website http://wwwabi.snv.jussieu.fr/public/abgd/abgdweb.html. The default values of Pmin =

178  0.001 and Pmax = 0.10, steps = 10 and number of intervals = 20 were used. Using the relative

179  gap width value (X) = 1.0 and correcting the distance matrix under the K80 Kimura model with a

180  MinSlope = 1.5.

181      The multi-rate Poisson Tree Process (mPTP), which is another single locus analysis, was

182  also used. This model incorporates different levels of intraspecific genetic diversity derived from

183  differences in the evolutionary history or in the sampling of each species, accommodating

184  different coalescence rates within the lineages (Kapli et al., 2017). mPTP analysis was performed

185  in a ML tree reconstructed by IQtree in CIPRES with the *COI* dataset (Suppl Fig. 1). For this

186  analysis the command line version of the mPTP v 0.2.4. software was used without considering

187  the outgroup. Four independent runs of 5,000,000 Monte Carlo Markov chains (MCMC) were

188  carried out sampling every 10,000 generations.

189     The use of these discovery methods leads to the Primary Species Hypothesis (PSH), used

190  as starting point for the validation step.

191     For the validation step, a Bayesian multilocus method of delimiting species (Yang &

192  Rannala, 2010, Yang & Rannala, 2014) implemented in the BPP v3.3 software (Yang, 2015) was

193  applied. Different hypotheses of species delimitation and estimation of the posterior probability

194  (PP) of each model were tested using reversible jump MCMC (rjMCMC). The previous species

195  assignment resulting from the ABGD discovery analysis was used as a starting hypothesis for the

196    BPP analysis, because it was the analysis that gave the largest number of PSHs. Some species

197    were excluded from this validation analysis since only one individual was available for each one

198    (*Cratera arucuia* Lago-Barcia & Carbayo, 2018 and *Cratera picuia* Lago-Barcia & Carbayo,

199    2018) or because it only had COI gene sequenced (*Cratera ochra* Rossi et al., 2016) . As they

200    were not the target species for our study, their removal from the analysis was not relevant. A

201    guide tree generated by 100 million generations (stored every 5000) in * BEAST2 v2.5.2

202    (Bouckaert et al., 2014) was built in CIPRES with the six single gene datasets (*BPP* datasets),

203    applying the evolutionary model for each gene resulting from the previous jmodeltest analysis

204    (18S=GTR+I; 28S=HKY+I+G; Cox1=GTR+G; EF=GTR+I+G; Nd4toCox1=HKY+I+G and

205    Tnuc=GTR+I).

206         The molecular clock was set as log normal relaxed for all markers (unlinked) and the

207    Birth and Death model was used for speciation. In the BPP analysis, both the size of the ancestral

208    population (theta, $\theta$) and the time of origin for each species (tau, $\tau$) were parameterized with four

209    different models (named M1-M4): M1 for large ancestral population size and deep divergence G

210    (1, 10) (for $\theta$ and $\tau$); M2 for small ancestral population size and shallow divergence G (2, 1000)

211    (for $\theta$ and $\tau$); M3 for large ancestral population size and shallow divergence (G (1 10) for $\theta$ and

212    G (2 1000) for $\tau$); and M4 for small ancestral population size and deep divergence (G (2 1000)

213    for $\theta$ and G (1 10) for $\tau$). Under the algorithm 0 it was run the rjMCMC analysis in 100,000

214    generations (with a sampling interval of 2) excluding 10% as burn-in. To test the robustness of

215    the results, these executions were replicated using different starting seeds. These analyses were

216    done without outgroup. Results of BPP lead to the Secondary Species Hypothesis (SSH).

217

218         **Abbreviations used in figures**

219     (cg) cyanophil gland cells

220     (co) common glandular ovovitelline duct

221     (e) eye

222     (ed) dilatated portion of ejaculatory duct

223     (ej) ejaculatory duct

224     (ep) esophagus

225     (fa) female atrium

226     (fc) female genital canal

227     (fo) fold

228     (g) gonopore

229     (gl) glands

230     (i) intestine

231     (lc) longitudinal cutaneous muscle fibers

232     (m) muscle fiber

233     (ma) male genital atrium

234     (mc) common muscle coat

235     (mo) mouth

236     (o) ovary

237     (ov) ovovitelline duct

238     (ph) pharyngeal pouch

239     (pb) penis bulb

240     (pp) penis papilla

241     (px) pharynx

242   (sb) subintestinal transverse muscle fibers

243   (sd) sperm duct

244   (sg) shell glands

245   (sp) supraintestinal transverse muscle fibers

246   (t) testis

247   (vi) vitellaria

248   (vn) ventral nerve plate

249

## Results

### Molecular datasets

252   The *COI* dataset consists of 40 sequences with a length of 822 bp, and the concatenated

253 dataset (28 *Cratera* sequences plus 3 outgroups from the genus *Obama*) has a length of 5671 bp.

254 The individual gene datasets for the *BEAST analysis are constituted by 26 sequences with a

255 length of 1349 bp (18S), 1544 bp (28S), 825 bp (COI), 612 bp (EF), 730 bp (Nd4toCox1) and

256 611 bp (Tnuc813).

257

### Phylogenetic analysis

259   The partitions obtained with PartitionFinder and applied to the phylogenetic analysis of

260 the *concatenated* dataset are Cox1_codon2, EF_codon2, 18S, Tnuc813-1_codon3, Tnuc813-

261 3_codon2, Tnuc813-3_codon3, Tnuc813-5_codon1, Tnuc813-5_codon2, Tnuc813-5_codon3 =

262 K81UF + G, 28S = TIM + G, Cox1_codon1, EF_codon1 = TRN + G, Cox1_codon3 = GTR + G,

263 EF_codon3, Tnuc813-1_codon2, Tnuc813-3_codon1 = TVM + G, Nd4toCox1-1_codon1,

264 Nd4toCox1-1_codon2, Nd4toCox1-3_codon1, Nd4toCox1-3_codon3, Tnuc813- 1_codon1 =

265 GTR + G, Tnuc813-2, Tnuc813-4 = GTR + G, Nd4toCox1-1_codon3, Nd4toCox1-2,

266  Nd4toCox1-3_codon2 = HKY + G. For the concatenated analyses, the topology obtained is the

267  same in both methods (ML and BI) as shown in Fig. 2. There is only a small difference in the

268  relationships between the specimens within two of the new species described in the present paper

269  (*Cratera piguaiatui* sp. nov. and *C. piguaiassu* sp. nov.), but without statistical support for any of

270  the two methods. All known species are monophyletic. The new species described here (*C.*

271  *piguaiatui* sp. nov., *C. imbiri* sp. nov. and *C. paraitinga* sp. nov.) are sister species, forming a

272  large monophyletic group, which in turn is sister to the species *C. cuarassu* Carbayo & Almeida,

273  2015. *Cratera pseudovaginuloides* (Riester, 1938) is a sister lineage of the new species described

274  here, *C. piguaiaboja* sp. nov., both constituting the sister group of a large clade formed by the

275  species *C. piguaiassu* sp. nov. and *C. crioula* (Froehlich, 1955) on the one hand and the group

276  constituted by the three species *C. picuia*, *C. arucuia* and *C. tamoia* (Froehlich, 1955). The vast

277  majority of the relationships present high support values at the nodes for both methodologies (PP

278  and bootstrap values).

279

280  **Molecular species delimitation**

281      On the concatenated tree in Fig. 2 is displayed a summary of the species delimitation

282  results. The ABGD method delimits within the *Cratera* genus 13 Molecular Operational

283  Taxonomic Units (MOTUs) with a p-value of P 0.001 - 0.0046.  The mPTP method delimits 11

284  candidate species for the ingroup with average support of 0.90. In both delimitations, mPTP and

285  ABGD, *C. ochra* is delimited as a single candidate species. However, it is not present in the

286  concatenated tree in Fig. 2 because there are only COI sequences in GenBank for this species

287  (Table 1 and Suppl Fig. 1). For this same reason the species is not included in the BPP analyses.

288      ABGD predicts a higher number of candidate species than mPTP. In consequence,

289   ABGD candidate set of species is adopted as a reference to designate the PSHs in order to test as

290   many scenarios as possible in the validation with the BPP method. The assignment is as follows.

291   All known species are delimited by both ABGD and mPTP methods as candidate species. Hence,

292   each is assigned a PHSs (PSH-4 is *C. cuarassu*, PSH-5 is *C. crioula*, PSH-8 is *C. tamoia* and

293   PSH-10 corresponds to *C. pseudovaginuloides*). Regarding the rest of *Cratera* individuals

294   included in this work, the two discovery methods coincide in assigning individuals F2789,

295   F2809, F5178 F2040, F2031, F2054 to one candidate species (PSH-1) and individuals F2828 and

296   F2829 to another candidate species (PSH-9). Finally, in two cases a clade that mPTP considers

297   as a single MOTU is divided in two candidate species by ABGD these are designated as

298   candidate species PSH-2, PSH-3, PSH-6 and PSH-7. The species *C. picuia* and *C. arucuia* are

299   not assigned any PSH because they are singletons (constituted by a single individual) and so are

300   not included in the validation step. So, finally 10 PSHs are set to be validated in BPP.

301        The species tree resulting from the *BEAST analysis (Fig. 3), used as the input tree to

302   implement the BPP method, differs slightly from the tree inferred using the concatenated dataset.

303   In the ML and BI phylogenies inferred from the concatenated dataset (Fig. 2), the clade formed

304   by PSH-9 and PSH-10 is sister to the clade constituted by PSH-5, PSH-6, PSH-7 and PSH-8.

305   However, in the *BEAST tree PSH-9 + PSH-10 is sister group of the rest of species. The small

306   differences could be due to the fact that *C. picuia* and *C. arucuia* were not included in the

307   *BEAST analysis, but this does not affect the subsequent species assignment.

308        The different values of $\theta$ (ancestral population size) and $\tau$ (time of divergence) that are

309   used in the 4 BPP analyses (M1, M2, M3 and M4) do not have a significant effect on the results

310   of the BPP analyses (Fig. 3), except for the node that separates PSH-2 and PSH-3, the PP value

311   of which is higher than 0.95 in the M2 and M4 models (small ancestral population size) and a

312    little lower than 0.95 in the M1 and M3 models (large ancestral population size). Of the 10 PSHs

313    that are analysed as starting hypothesis for BPP, only 9 are validated since PSH-6 and PSH-7

314    would form a single SSH (SSH-6 in Fig. 3). In conclusion, the BPP results determine the

315    presence of 9 SSHs, validating five new species of *Cratera* (SSH-1, SSH-2; SSH-3, SSH-6, and

316    SSH-9) that will be described in the following section.

317

318    **Taxonomic account**

319    **Order Tricladida Lang, 1884**

320    **Suborder Continenticola Carranza et al., 1998**

321    **Family Geoplanidae Stimpson, 1857**

322    **Genus *Cratera* Carbayo et al., 2013**

323

324    ***Cratera piguaiassu* sp. nov., Araujo, Carbayo, Riutort & Álvarez-Presas**

325    urn:lsid:zoobank.org:act:DE3D812D-C387-40BD-9273-7BC1FE59D09C

326

327    **Synonymy.**

328    *Cratera* sp. 1: Carbayo et al. (2013).

329    **Etymology.** The name *piguaiassu* is a free composition of the Tupi (indigenous Brazilian

330    language) words pyguaia (meaning hole, cave) and assu (meaning large) (Tibiriçá, 1984). It

331    refers to the large distal dilatation of the ejaculatory duct.

332    **Type locality.** Parque Nacional da Serra da Bocaina, São José do Barreiro, State of São Paulo,

333    Brazil.

334    **Material studied.** All specimens collected in the Parque Nacional da Serra da Bocaina, São José

335    do Barreiro, State of São Paulo, Brazil (-22.75, -44.62) by Carbayo et al. Holotype F2825

336    (MZUSP PL 2150): 8 September 2008. Horizontal sections of pre-pharyngeal region-1 on 5

337    slides; transverse sections of pre-pharyngeal region-2 on 5 slides; sagittal sections of pharynx

338    and copulatory apparatus on 34 slides. Paratypes: F2025 (MZUSP PL 2146): 5 February 2008.

339    Horizontal sections of pre-pharyngeal region-1 on 15 slides; transverse sections of pre-

340    pharyngeal region-2 on 7 slides. Sagittal sections of copulatory apparatus on 15 slides. F2807

341    (MZUSP PL 1050): 7 September 2008. Transverse sections of cephalic extremity on 7 slides;

342    horizontal sections of ovaries on 5 slides; transverse sections of pre-pharyngeal region on 6

343    slides; sagittal sections of pharynx on 12 slides; sagittal sections of copulatory apparatus on 11

344    slides. F2821 (MZUSP PL 1052): 8 September 2008. Sagittal sections of a piece of the body

345    behind cephalic extremity on 71 slides; sagittal sections of pharynx and copulatory apparatus on

346    71 slides. F2834 (MZUSP PL 2151): 8 September 2008. Preserved in 80% ethanol.

347    **Diagnosis**

348         Species of *Cratera* 50-62 mm long (34-38 mm preserved); dorsum chestnut brown to

349    black brown, excepting the yellow orange or grayish body margins. A thin grayish median stripe

350    may be present. Eyes dorsal. Pharynx bell-shaped. Penis papilla horizontal; distal portion of

351    ejaculatory duct very dilated to occupy most of the length of the penis papilla. Common

352    glandular ovovitelline duct absent.

353    **Description**

354         When crawling, the longest specimen (paratype F2807), up to 62 mm in length and 3.5

355    mm in width; preserved, 38 and 7 mm, respectively. Body elongate, slightly lanceolated, with

356    maximum width at the level of the pharynx. Anterior to it, body narrows gradually towards the

357    rounded tip; posterior to the level of the pharynx, body becomes narrower abruptly near

358  posterior, pointed tip. Dorsum slightly convex, ventral side flattened. Creeping sole as wide as

359  92-94% of body width at the pre-pharyngeal region. Mouth at a distance from anterior extremity

360  equal to 70% of body length; gonopore at 85 % in holotype. In paratype F2807, 74% and 85%,

361  respectively.

362      Color of the dorsum varies from chestnut brown (Fig. 4A) to black brown (Fig. 4B). A

363  submarginal yellow orange or grayish stripe is present in anterior tenth of the body; posteriorly,

364  this stripe becomes marginal. The stripe, measuring 8% of body width, may be inconspicuous. A

365  thin grayish median stripe, 4% of body width, may also occur. Ventral surface varies from deep

366  orange (Fig. 4A, inset) to grayish (Fig. 4B, inset).

367      Each eye is formed by a single pigmented cup 30 μm in diameter. Clear halos around

368  eyes were not observed. Eyes contour anterior extremity of the body in a single row along the

369  first 5 millimeters (equal to 13% of body length, paratype F2807); then they spread onto the back

370  in a lateral band 1/3th of the body width, reaching the posterior tip.

371      Sensory pits, 15 μm deep, in a uniserial ventro-lateral row, from very anterior tip up to

372  29% of body length posterior. Dorsal and ventral epidermis in pre-pharyngeal region pierced by

373  necks of two types of cell glands producing erythrophil and cyanophil granules, respectively.

374  Besides, rhabditogen cells discharge their content through dorsal epithelium. Glandular margin

375  constituted by two types of cell glands, one abundant type producing xanthophil granules and a

376  less abundant type secreting erythrophil granules.

377      Cutaneous musculature constituted of a subepithelial circular layer, followed by two

378  diagonal layers with decussate fibers, and then a strongly developed longitudinal layer with

379  fibers arranged in bundles (Fig. 4C). Longitudinal layer is 40 μm thick dorsally and 50 μm

380  ventrally (paratype F2807); dorsally, fibers gathered into well-delimited and more compact

381     bundles than ventrally. Thickness of cutaneous muscle ranges from 8.9% (F2807) to 13.4%

382     (F2025).

383         Three parenchymal muscle layers throughout the body: a dorsal layer of diagonal

384     decussate fibers (20 μm thick), a transverse supraintestinal layer (150 μm), and a transverse

385     subintestinal one (90 μm). Central nervous system as a ventral nerve plate. Cerebral ganglia were

386     not discerned.

387         Mouth located shortly behind middle of pharyngeal pouch. Pharynx bell-shaped, with

388     dorsal insertion posterior to the ventral at the equivalent of 40% of pharyngeal length (Fig. 4D).

389     Esophagus length, 33% of pharyngeal length. Outer pharyngeal epithelium underlain by a one-

390     fiber-thick layer of longitudinal muscle, followed by a circular one (7 μm thick); inner

391     epithelium underlain by a layer (70-150 μm) of circular fibers with interspersed longitudinal

392     fibers, followed by a longitudinal muscle layer (10 μm). Pharyngeal pouch at 1.6-2.6 mm from

393     prostatic vesicle.

394         Testes dorsal, located under the supraintestinal transverse muscle layer, partially placed

395     between the intestinal diverticula (Fig. 4C). Sperm ducts run immediately above the subintestinal

396     muscle layer, dorso-medially to the ovovitelline ducts (Fig. 4C). Shortly behind the prostatic

397     vesicle, sperm ducts curve medially and anteriorly, to communicate separately with the

398     respective short lateral diverticulum of the vesicle (Fig. 5A). Vesicle extrabulbar, tubular, with

399     anterior portion slightly dilated. In lateral view vesicle with the shape of an inverted U, the distal

400     portion of which, anterior to anterior region of penis bulb, communicates with ejaculatory duct.

401     Prostatic vesicle lined with a ciliated, tall and tortuous epithelium, which is traversed by cells

402     producing fine erythrophil granules. This epithelium surrounded by a circular muscle layer.

403     Ejaculatory duct straight, running slightly dorsally. At the basis of the penis papilla, duct widens

404  to give rise to a very large cavity inside the penis papilla (Figs. 5A-C). At the tip of penis papilla

405  this cavity narrows to open into male atrium. Ejaculatory duct lined with a cuboidal, ciliated

406  epithelium and surrounded by a 25-μm thick circular muscle layer. Under this muscle layer,

407  there is an additional, one-fiber-thick layer of longitudinal muscle.

408      Penis papilla a long, roughly conical, protrusible organ extending along the length of the

409  male atrium or even beyond (Fig. 5A-C). Lining epithelium of the penial cavity cuboidal, not

410  ciliated, pierced by necks of cell producing minute erythrophil granules (<0.2 μm), and underlain

411  by a layer (25 μm) of circular muscle, followed by a simple layer of longitudinal muscle. The

412  penis papilla is clothed with a cuboidal, non-ciliated epithelium, which is traversed by necks of

413  cells producing erythrophil granules and is underlain by a 20-μm-thick layer of circular muscle

414  with some interspersed longitudinal fibers.

415      Male atrium ample and smooth, not narrowed distally. It is lined with a cuboidal, non-

416  ciliated epithelium, which is pierced by necks of cells producing granules with weak xanthophil

417  affinity. Male atrial epithelium underlain by a muscle layer (40 μm) of circular fibers.

418      Ovaries roughly ovoid, with maximum length 400 μm anteroposteriorly. They are located

419  immediately above the ventral nerve plate, at a distance from anterior tip equivalent to 21% of

420  body length. Ovovitelline ducts arise from external side of the ovaries, subsequently run

421  backwards above ventral nerve plate. The ducts ascend laterally to the female atrium, posteriorly

422  and medially inclined, to unite dorsally to the atrium (Fig. 5A). Half of the ascending portion of

423  these ducts receives secretion of shell glands. Ovovitelline ducts open the female genital canal.

424  This canal is a long canalicular projection of the posterior portion of the female atrium. This

425  canal is directed forwards (Fig. 5D). Female atrium, as long as male atrium, and funnel-shaped.

426  Lateral walls of female atrium partially occlude its lumen. Its lining epithelium is columnar, and

427  the free surface of which is erythrophil and displays small recesses that appear as small gaps. In

428  the anterior portion of female atrium, the epithelium is 40 μm high; posteriorly it becomes taller

429  and its nuclei arranged at different heights within the cells, so giving to the epithelium a

430  multilayered aspect. Necks of cells producing erythrophil granules pierce this epithelium, which

431  is clothed with two layers of muscles; clothing the anterior half of the atrium there is a 5-μm-

432  thick circular muscle layer followed by a 3-μm-thick longitudinal one. Arrangement of these

433  layers is inverted in posterior half of female atrium, i. e., a layer (5 μm) of longitudinal is

434  followed by a layer (20 μm) of circular fibers.

435  **Remarks**

436       Regarding the external aspect, *C. tamoia* is the only species of the genus resembling *C.*

437  *piguaiassu* in that both display a uniform dark dorsum with clear margins. However, although

438  color patterns are alike, *C. piguaiassu* differs in being darker. Moreover, the phylogenetic

439  analyses show that these two species are highly differentiated at the genetic level and do not even

440  represent sister groups. Regarding the internal organs, *C. piguaiassu* is unique among the

441  representatives of *Cratera* in the very large dilatation of the ejaculatory duct. This dilatation

442  occupies most of the penis papilla. This situation is also present in *C. cuarassu*, but the penis

443  papilla of the latter is vertically oriented (vs. horizontally in *C. piguaiassu*). The molecular

444  delimitation methods all clearly point to *C. piguaiassu* being a species differentiated from the

445  rest of species molecularly analysed in the present study. On the other hand, although the

446  primary hypothesis found this lineage could be divided in two species, neither the molecular

447  validation nor the morphological analysis found evidence of this possibility.

448

449  ***Cratera piguaiaboja* sp. nov., Araujo, Carbayo, Riutort & Álvarez-Presas**

450     urn:lsid:zoobank.org:act:46D76DD7-B129-461D-8803-3E918AA4601C

451

452     **Etymology.** The name *piguaiaboja* is a free composition of the Tupi (indigenous Brazilian

453     language) words pyguaia (meaning hole, cave) and bojá (meaning intermediate, middle)

454     (Tibiriçá, 1984). It refers to the middle size of the distal dilatation of the ejaculatory duct.

455     **Type locality.** Parque Nacional da Serra da Bocaina, São José do Barreiro, State of São Paulo,

456     Brazil.

457     **Material studied.** All specimens collected in Parque Nacional da Serra da Bocaina, São José do

458     Barreiro, State of São Paulo, Brazil (-22.75, -44.62), in September 2008 by Carbayo et al.

459     Holotype F2829 (MZUSP PL 0459): transverse sections of cephalic extremity on 4 slides;

460     horizontal sections of a portion of the body behind cephalic extremity on 4 slides; transverse

461     sections of pre-pharyngeal portion on 7 slides; sagittal sections of pharynx on 6 slides; sagittal

462     sections of copulatory apparatus on 4 slides (plus one slide lost). F2828 (MZUSP PL 0458):

463     horizontal sections of a portion behind anterior extremity on 6 slides; transverse sections of the

464     pre-pharyngeal portion on 22 slides; sagittal sections of pharynx on 13 slides; sagittal sections of

465     copulatory apparatus on 14 slides.

466     **Diagnosis**

467         Species of *Cratera* 34 mm long preserved; dorsum olive grey with large black dots, with

468     these being more concentrated in paramedian bands; eyes marginal; pharynx bell-shaped; distal

469     portion of ejaculatory duct dilatated to occupy half of the penis papilla; male atrium separated

470     from female by a narrowing; penis papilla shorter than male atrium; prostatic vesicle with

471     inverted-U shape in lateral view; penis papilla postero-dorsally oriented; numerous cyanophil

472     cell necks piercing roof of male atrium; female atrium half the length of the male atrium;

473    common glandular ovovitelline duct absent.

474    **Description**

475         Fixed, holotype measures 34 mm in length and 4 in width. Body elongate, with parallel

476    margins along most of body length. Anterior extremity rounded; posterior pointed. Dorsal side

477    convex; ventral side flattened. Creeping sole, 95% of body width at the pre-pharyngeal region.

478    Mouth at a distance from anterior extremity equal to 71% of body length; gonopore at 87%

479    (holotype).

480         Dorsum spotted black on olive grey ground color (Fig. 6A-D). Large black spots join

481    each other. Spots distributed all over dorsum and especially concentrated in a median band (33%

482    of body width). This band may be divided by a thin midline, measuring 6% of body width (Fig.

483    6C). Ventral surface olive gray (Fig. 6A), gray at anterior extremity.

484         Each eye is formed by a single pigmented cup 40 µm in diameter. Clear halos around

485    eyes were not found. Eyes contour anterior extremity in a single row, posteriorly they are

486    arranged marginally until posterior tip of the body.

487         Sensory pits were not found despite intensive search on the sections, which are partially

488    damaged. Dorsal and ventral epidermis in pre-pharyngeal region pierced by necks of two types

489    of cell glands producing granules, erythrophil and cyanophil, respectively. Besides, rhabditogen

490    cells discharge their content through dorsal epithelium and, scarcely, ventral epithelium as well.

491    Glandular margin not well defined (Fig. 7A), constituted by three types of cell glands, one

492    abundant type producing xanthophil granules and a less abundant type secreting erythrophil

493    granules, and rhabditogen cells.

494         Cutaneous musculature constituted of a subepithelial circular layer, followed by two

495    diagonals with decussate fibers, and then a strongly developed longitudinal layer with fibers

496    arranged in bundles (Fig. 7A). Longitudinal layer 55 μm thick dorsally and 90 μm ventrally.

497    Fibers of this layer are gathered into well-delimited and more compact bundles than ventrally.

498    Thickness of cutaneous muscle, 12.5% of body height (holotype).

499         Three parenchymal muscle layers throughout the body: a dorsal layer of diagonal

500    decussate fibers (20 μm thick, holotype), a transverse supraintestinal layer (60 μm), and a

501    transverse subintestinal one (70 μm). Central nervous system as a ventral nerve plate. Cerebral

502    ganglia starting at 0.5 mm from anterior extremity (1.5% of body length, holotype).

503         Mouth located at the end of second third of pharyngeal pouch (Fig. 7B). Pharynx bell-

504    shaped, with dorsal insertion posterior to the ventral at the equivalent of 36% of pharyngeal

505    length. Esophagus length, 21% of pharyngeal length. Outer pharyngeal epithelium underlain by a

506    one-fiber-thick longitudinal muscle layer followed by a circular one (4 μm thick); inner

507    epithelium underlain by a circular muscle layer (30-60 μm thick), followed by a longitudinal

508    muscle one (5 μm). Pharyngeal pouch of holotype at 2.5 mm (equivalent to 7% of body length)

509    from prostatic vesicle.

510         Testes dorsal, located under the supraintestinal transverse muscle layer, partially placed

511    between the intestinal diverticula (Fig. 7A). Posteriormost testes lateral to insertion of the

512    pharynx. Sperm ducts run immediately above the subintestinal muscle layer, dorso-medially to

513    the ovovitelline ducts (Fig. 7A). Below prostatic vesicle, sperm ducts curve medially and

514    anteriorly, to communicate separately with the respective short lateral diverticulum of the

515    vesicle. Prostatic vesicle extrabulbar and tubular. In lateral view, this vesicle is seen as an

516    inverted U. Prostatic vesicle approaches anterior region of penis bulb and communicates with

517    ejaculatory duct. Ventral portion of penis bulb posterior to dorsal portion.

518         Prostatic vesicle lined with a ciliated, columnar epithelium, traversed by necks of two

519    types of cell producing erythrophil and cyanophil granules, respectively, the cyanophil glands

520    being much more abundant (Fig. 8A). Epithelium of prostatic vesicle surrounded by a 130-µm-

521    thick circular muscle layer. Proximal portion of ejaculatory duct sinuous; distal portion straight,

522    traversing center of penis papilla; midway of penis papilla, ejaculatory duct widens to give rise to

523    a relatively large, funnel-shaped cavity, which opens at the tip of the penis papilla (Fig. 7C-D,

524    8A). Ejaculatory duct lined with a cuboidal, ciliated epithelium; in its dilatated portion, pierced

525    by necks of cells producing xanthophil granules. Epithelium of ejaculatory duct surrounded by a

526    20-µm thick circular muscle layer.

527        Penis papilla conical cylindrical, 1.3-1.5 times longer than its diameter and as long as the

528    male atrium or shorter (Fig. 7C-D). Penis papilla clothed with non-ciliated epithelium. Columnar

529    epithelium lines basal half of papilla; cuboidal epithelium lines distal half. Epithelium of papilla

530    pierced by necks of three types of cells producing erythrophil, xanthophil and cyanophil

531    granules, respectively (but the latter appears erythrophil in paratype); necks of cyanophil glands

532    only piercing epithelium of basal half of penis papilla. Epithelium of penis papilla underlain by a

533    10-µm-thick layer of circular muscle fibers followed by a longitudinal layer, 10 µm thick.

534    Parenchyma of penis papilla richly traversed by circular and longitudinal muscle fibers.

535        Male atrium ample and smooth, lined with a columnar, non-ciliated epithelium.

536    Epithelium clothing roof of male atrium pierced by very numerous necks of cells producing

537    cyanophil granules. Ventral portion of male atrium pierced by necks of glands producing

538    erythrophil granules. Atrial epithelium underlain by a layer (12 µm thick) of circular muscle

539    fibers, followed under dorsal epithelium by a 5-µm-thick longitudinal muscle layer.

540        Ovaries were not found in histological sections and were probably destroyed in the

541    portion from which a tissue sample was extracted. Ovovitelline ducts ascend laterally to

542    proximal portion of the female atrium, posteriorly and medially inclined. Subsequently, the ducts

543    unite dorsally to the posterior portion of atrium. Half of ascending portion of these ducts receives

544    shell glands. Ovovitelline ducts open into female genital canal, i.e., a common glandular

545    ovovitelline duct is absent. Female genital canal projects forwards from the postero-dorsal

546    portion of the female atrium. Female atrium ample, 55-57% the length of male atrium and lined

547    with 30-70 μm high, non-ciliated epithelium, with stratified aspect. Surface of epithelium

548    sinuous; subapical portion of epithelial cells cyanophil (Fig. 8B) or erythrophil Fig. 8C). Necks

549    of two types of cells, producing erythrophil and cyanophil granules, respectively, pierce this

550    epithelium, which is underlain by a 25-μm thick and dense layer of circular muscle, followed by

551    a 3 μm thick longitudinal muscle layer.

552    **Remarks**

553         *C. piguaiaboja* is distinctive among all species of the genus in the spotted color pattern of

554    the dorsal side. Regarding its copulatory apparatus, there are five species with a similar aspect of

555    the copulatory apparatus and size of the dilatation of the ejaculatory duct, namely, *C.*

556    *aureomaculata* Rossi & Leal-Zanchet, 2017, *C. nigrimarginata* Rossi & Leal-Zanchet, 2017, *C.*

557    *pseudovaginuloides*, *C. tamoia*, and *C. viridimaculata* Negrete & Brusa, 2016. However, (a) all

558    of these five species have a common glandular ovovitelline duct (vs. absent in *C. piguaiaboja*;

559    but see redescription of *C. pseudovaginuloides* in Riester, 1938); (b) the male and female atria

560    are not separated by a constriction in *C. pseudovaginuloides* (vs. separated in *C. piguaiaboja*);

561    (c) the penis papilla is longer than the male atrium in *C. nigrimarginata* and *C.*

562    *pseudovaginuloides* (vs. shorter in *C. piguaiaboja*); (d) the prostatic vesicle is horizontal in *C.*

563    *nigrimarginata* (vs. inverted-U shaped in *C. piguaiassu*); (e) the female atrium is funnel-shaped,

564    and its posterior section oriented upwards in *C. viridimaculata* (vs. horizontal, and not funnel-

565   shaped in *C. piguaiaboja*); (f) the prostatic vesicle runs postero-dorsally in *C. aureomaculata*

566   and *C. tamoia* (vs. inverted U-shaped in *C. piguaiaboja*); (g) the penis papilla exhibits a postero-

567   ventral orientation in *C. tamoia* (vs. postero-dorsal in *C. piguaiaboja*); and (h) there is no

568   accumulation of necks of cyanophil cells piercing the roof of the male atrium in *C.*

569   *nigrimarginata*, *C. pseudovaginuloides*, and *C. tamoia* (vs. present in *C. piguaiaboja*).

570          The phylogenetic tree as well as the molecular species delimitation analyses also show

571   that this species is distinct and well-delimited from *C. pseudovaginuloides* and *C. tamoia*, the

572   two species included in these analyses that show similarities with *C. piguaiaboja*.

573

574   ***Cratera piguaiatui* sp. nov., Araujo, Carbayo, Riutort & Álvarez-Presas**

575   urn:lsid:zoobank.org:act:FB96BE96-86AD-41FB-961F-C0337C56A596

576

577   **Synonymy.** *Cratera* sp. 4: Carbayo et al. (2013).

578   **Etymology.** The name *piguaiatui* is a free composition of the Tupi (indigenous Brazilian

579   language) words pyguaia (meaning hole, cave) and tui (meaning tiny, insignificant) (Tibiriçá,

580   1984). It refers to the small distal dilatation of the ejaculatory duct.

581   **Type locality.** Parque Nacional da Serra da Bocaina, São José do Barreiro, State of São Paulo,

582   Brazil.

583   **Distribution.** Parque Nacional da Serra da Bocaina, São José do Barreiro, State of São Paulo;

584   Parque Nacional Itatiaia, Resende, State of Rio de Janeiro, Brazil.

585   **Material studied.** Holotype F2809 (MZUSP PL 1051): Parque Nacional da Serra da Bocaina,

586   São José do Barreiro, State of São Paulo (-22.75, -44.62). F. Carbayo et al., 7 September 2008;

587   transverse sections of cephalic extremity on 4 slides; sagittal sections of a portion immediately

588 behind cephalic extremity on 19 slides; horizontal sections of a immediately behind on 12 slides;

589 transverse sections of pre-pharyngeal on 16 slides; sagittal sections of pharynx on 17 slides;

590 sagittal sections of copulatory apparatus on 23 slides. Paratypes: F2031 (MZUSP PL 1014):

591 Ibidem, 7 September 2008; sagittal sections of copulatory apparatus on 6 slides. F2054 (MZUSP

592 PL 2148): Ibidem, 9 September 2008; sagittal sections of pharynx and copulatory apparatus on

593 13 slides (including 3 slides lost). F2040 (MZUSP PL 2147): Ibidem, 9 February 2007,

594 preserved in 80% ethanol. F2798 (MZUSP PL 2149): Ibidem, 7 September 2008; preserved in

595 80% ethanol. F5178 (MZUSP PL 2154): Parque Nacional de Itatiaia, Resende, State of Rio de

596 Janeiro (-22.43328, -44.61539), Brazil, F. Carbayo et al., 5 April 2012, horizontal sections of a

597 body portion behind cephalic extremity on 7 slides; transverse sections of pre-pharyngeal on 15

598 slides; sagittal sections of pharynx on 17 slides; sagittal sections of copulatory apparatus on 30

599 slides.

600 **Diagnosis**

601 Species of *Cratera* 45-70 mm long preserved; dorsum with a melon yellow median stripe,

602 bordered on either side by a jet-black stripe external to which a marginal traffic white stripe;

603 body margins jet black. Anterior 1/5th of the body colored with a gradient of carmine red; eyes

604 marginal; pharynx cylindrical; distal dilatation of ejaculatory duct relatively small; pharyngeal

605 pouch 0.6 mm anterior to the prostatic vesicle (equal to 1% of body length); penis papilla shorter

606 than male atrium; female atrium 2.5 times longer than the male atrium; common glandular

607 ovovitelline duct long.

608 **Description**

609 Preserved 45-58 mm in length and 7 mm in width. Body slightly lanceolate, with

610 maximum width at the level of the pharynx. Anterior to it, body becomes thinner gradually to the

611    rounded tip; posterior to the level of the pharynx, body becomes thinner abruptly close to

612    posterior pointed tip. Dorsum slightly convex, ventral side flattened. Creeping sole, 95% of body

613    width at pre-pharyngeal region. Mouth at a distance from anterior extremity equal to 73% of

614    body length; the gonopore at 82% (holotype).

615         Dorsum with a melon yellow median stripe, 28% of body width, which is bordered on

616    either side by a jet-black stripe, 22% of the body width (Fig. 9A-B). External to jet black stripes,

617    a traffic white marginal stripe, 10% of body width; body margin (3% of the body width) jet

618    black. Anterior 1/5th of the body colored with a gradient of carmine red, dorsally and ventrally;

619    otherwise, ventral side grey white (Fig. 9B).

620         Each eye is formed by a single pigmented cup with 35 µm in diameter. No clear halos

621    around eyes. Eyes contour the anterior extremity in a single row and extend marginally until

622    posterior tip.

623         Sensory pits, 20 µm deep, as a uniserial ventro-lateral row, from anterior extremity

624    through a body length at least equal to 9% of body length (holotype). Besides rhabditogen cells,

625    necks of two types of cell glands, producing xanthophil and erythrophil granules, respectively,

626    pierce prepharyngeal dorsal epithelium; the latter also pierce ventral epithelium. Conspicuous

627    glandular margin constituted of abundant glands producing erythrophil granules (Fig. 10A).

628         Cutaneous musculature of three layers: a subepithelial circular layer, followed by two

629    diagonals with decussate fibers, and then a strongly developed longitudinal, 30 µm thick dorsally

630    and 40 µm thick ventrally (holotype). Fibers of the longitudinal layer gathered in bundles which

631    are dorsally better delimited than ventrally. Relative thickness of cutaneous muscle, 9.1%

632    (holotype).

633         Three parenchymal muscle layers throughout the body, all constituted by fibers relatively

634 densely packed: a dorsal layer of diagonal decussate fibers (15 μm thick, holotype), a transverse

635 supraintestinal layer (25 μm), and a transverse subintestinal one (25 μm).

636       Central nervous system as a ventral nerve plate. Clearly evident cerebral ganglia were not

637 found.

638       Mouth in middle of pharyngeal pouch (Fig. 10B). Pharynx cylindrical, with dorsal

639 insertion posterior to the ventral at the equivalent of 20% of pharyngeal length (paratype F2054).

640 Esophagus length, ca. 10% of pharyngeal length (paratype F2054). Outer pharyngeal epithelium

641 underlain by a one-fiber-thick layer (4 μm) of longitudinal muscle fibers followed by a layer of

642 circular fibers (7 μm); inner pharyngeal epithelium underlain by a layer (80 μm) of circular

643 fibers, followed by a layer (10 μm) of longitudinal fibers (holotype). Pharyngeal pouch at 600

644 μm from prostatic vesicle in holotype (or 1% of body length).

645       Testes dorsal, located under supraintestinal transverse muscle layer, partially placed

646 between the intestinal diverticula. The testes extend from level of ovaries to nearly root of

647 pharynx. Distal course of sperm ducts running posteriorly and medially to communicate with the

648 respective lateral diverticulum of the prostatic vesicle (Fig. 11A). Paired portion represents ca.

649 half of the total length of this organ. This vesicle, extrabulbar, approximately pear-shaped in

650 lateral view, with posterior portion running posteriorly and upwards until anterior region of penis

651 bulb. Vesicle lined with a ciliated epithelium, which is pierced by necks of cells producing fine

652 erythrophil granules. A 20 μm thick layer of circular muscle fibers surrounds vesicle. Inside

653 penis papilla vesicle communicates with a horizontal, initially sinuous ejaculatory duct which is

654 lined with a cuboidal, ciliated epithelium. This epithelium surrounded by a 5 μm thick layer of

655 circular muscle fibers. Near tip of penis papilla, lumen of the ejaculatory duct doubles its width

656 to form a small cavity (Fig. 11A-C).

657   Penis papilla short, horizontally placed, and roughly bulb-shaped; shorter than male

658 atrium (Fig. 11A-B). Male atrium slightly folded. Penis papilla and male atrium clothed with a

659 cuboidal non ciliated epithelium, this pierced by necks of two types of cells, producing

660 erythrophil and xanthophil granules, respectively. Epithelium of penis papilla and that of male

661 atrium underlain by a 7-μm-thick layer of circular muscle fibers, followed by a 7-μm-thick layer

662 of longitudinal muscle fibers.

663   Ovaries elongate, roughly ovoid, with 250 μm anteroposteriorly. They are located

664 immediately above the ventral nerve plate, at a distance from anterior tip equivalent to 30% of

665 body length (holotype). Ovovitelline ducts arise from dorso-external side of ovaries and run

666 backwards above the ventral nerve plate. They ascend laterally to female atrium to unite

667 common glandular ovovitelline duct dorsally to female atrium. Distal ascending portion of these

668 ducts receive shell glands. Common glandular ovovitelline duct long (1.2 mm, ie., 1/3th of the

669 length of female atrium in holotype) communicating with female genital canal, the latter being a

670 projection of the posterior portion of female atrium directed forwards and dorsally. Female

671 atrium funnel-shaped, with a length 2.5 times that of male atrium. Lateral wall of female atrium

672 with folds narrowing its lumen. Female atrium lined with a non-ciliated, 25 μm tall epithelium

673 along anterior 4/5th of its length. Posterior 1/5th lined with a 50-μm-high epithelium that might

674 display a multilayered one; quality of the sections precluded confirmation. Necks of cells

675 producing erythrophil granules pierce female epithelium, this underlain by a layer of circular

676 muscle fibers (7 μm thick, holotype) followed by a layer of longitudinal fibers (7 μm thick).

677 **Remarks**

678   Among all species of the genus, only *C. taxiarcha* (Marcus, 1951) resembles *C.*

679 *piguaiatui* in the three-color striped pattern of the dorsum composed of white, yellow, and black

680    colors. However, in *C. taxiarcha*, the median stripe is white (vs. yellowish in *C. piguaiatui*).

681    Regarding the copulatory apparatus, all species in the genus possess a female atrium as long as

682    the male atrium, with minor variations whereas in *C. piguaiatui* it is 2.5 times longer. The

683    molecular delimitation methods all clearly point to *C. piguaiatui* being a species differentiated

684    from the rest of species molecularly analysed in the present study.

685

686    ***Cratera imbiri* sp. nov., Araujo, Carbayo, Riutort & Álvarez-Presas**

687    urn:lsid:zoobank.org:act:CC5B22EB-9E7C-490F-A6FF-03757BA03C26

688

689    **Etymology.** The name *imbiri* refers to Vila de São Matheus do Imbiri, former name of Campos

690    do Jordão, type locality of the species.

691    **Type locality.** Parque Estadual Campos do Jordão, Campos do Jordão, State of São Paulo,

692    Brazil.

693    **Distribution.** Type locality only.

694    **Material studied.** Holotype F5512 (MZUSP PL 2155): Parque Estadual Campos do Jordão,

695    Campos do Jordão, State of São Paulo, Brazil (-22.68878, -45.48068). F. Carbayo et al., 15

696    November 2012. Horizontal sections of a behind cephalic extremity on 7 slides; transverse

697    sections of pre-pharyngeal on 9 slides; sagittal sections of pharynx on 13 slides; sagittal sections

698    of copulatory apparatus on 9 slides.

699    **Diagnosis**

700       Species of *Cratera* 26 mm long preserved; dorsal median stripe sulfur yellow bordered

701    on either side by a khaki grey band; body margins cream; in anterior 1/4th of the body, this

702    pattern covered with a color gradient of coral red; eyes marginal; pharynx cylindrical, with

703    dorsal insertion posteriorly shifted at the equivalent of 20% the length of pharynx; pharyngeal

704    pouch 600 µm anterior to prostatic vesicle; paired portion of the prostatic vesicle with 1/3th of

705    total length of this organ; epithelium of penis papilla underlain by a layer of circular muscle

706    fibers only; female atrium 2.5 times longer than male atrium, female atrium narrows gradually

707    towards its posterior section; common glandular ovovitelline duct long.

708    **Description**

709            When creeping, body 38 mm long and 2.5 mm wide. Preserved 26 mm and 4 mm,

710    respectively. Body margins parallel along most of its length. Extremities of the body rounded.

711    The dorsum slightly convex, ventral side flattened. Creeping sole, 94% of body width at the pre-

712    pharyngeal region. Mouth at a distance from anterior extremity equal to 70% of body length;

713    gonopore, 78%.

714            Dorsal color with a sulfur yellow median stripe, 14% of the body width, this bordered on

715    either side by a khaki grey band, 34% of the body width. Body margins (9% of body width)

716    cream (Fig. 12A). In anterior 1/4th of body, this pattern covered with a gradient color of coral

717    red. Ventral side coral red along anterior 1/4th, and cream colored behind (Fig. 12B).

718            Eyes of one pigmented cup with 25 µm in diameter. No clear halos around eyes were

719    seen. Eyes contour the anterior extremity in a single row and extend marginally until posterior

720    extremity. Anterior extremity of body with 3mm long not available (used for DNA extraction).

721    Sensory pits, 20 µm deep, as a uniserial ventro-lateral row in along a body portion initiating 3

722    mm behind anterior tip of the body and extending backwards 3.7 mm. Necks of cell glands

723    producing erythrophil granules pierce dorsal and ventral epithelium in prepharyngeal region.

724    Besides, rhabditogen cells discharge their content through dorsal epithelium. Glandular margin

725    constituted of abundant glands producing erythrophil granules.

726    Cutaneous musculature of a subepithelial circular layer, followed by two diagonals with

727    decussate fibers, and then a strongly developed longitudinal, 35 μm thick dorsally and 30 μm

728    thick ventrally. Thickness of cutaneous muscle, 11.3% of body height in the pre-pharyngeal

729    region.

730    Three parenchymal muscle layers are present throughout the body: a dorsal layer of

731    diagonal decussate fibers (10 μm thick), a transverse supraintestinal layer (20 μm), and a

732    transverse subintestinal one (20 μm).

733    Central nervous system as a ventral nerve plate. Cerebral ganglia not discerned.

734    Mouth located at the end of the anterior half of pharyngeal pouch (Fig. 12C). Pharynx

735    cylindrical, with dorsal insertion posterior to the ventral at the equivalent of 7% of pharyngeal

736    length. Esophagus length, 20% of pharyngeal length. Outer pharyngeal epithelium underlain by a

737    one-fiber-thick layer of longitudinal muscle fibers followed by a layer of circular fibers (5 μm

738    thick); inner pharyngeal epithelium underlain by a layer of circular muscle fibers (60-100 μm),

739    followed by a layer of longitudinal fibers (8 μm). Pharyngeal pouch 80 μm anterior to prostatic

740    vesicle.

741    Testes dorsal, located under the supraintestinal transverse muscle layer, partially placed

742    between the intestinal diverticula. The testes extend from 200 μm behind the level of the ovaries

743    to 1 mm anterior to the root of pharynx. Sperm ducts very narrowed at the point of

744    communication with the respective branch of prostatic vesicle. Paired portion of this vesicle with

745    ca. 1/3rd of the total length of the organ. Prostatic vesicle extrabulbar, running postero-dorsally

746    until anterior region of penis bulb. Vesicle lined with a ciliated epithelium, this pierced by necks

747    of cells producing fine erythrophil granules. A 50-μm-thick circular muscle surround the vesicle.

748    Inside the penis papilla, vesicle communicates with the horizontal, sinuous ejaculatory duct. This

749    duct is dilatated distally at the tip of the penis papilla the equivalent of 2/5th of length of penis

750    papilla. Ejaculatory duct lined with a cuboidal, ciliated epithelium, its cilia being as long as cell

751    height, i.e., 10 µm. This epithelium surrounded by a 5-µm-thick layer of circular muscle fibers.

752          Penis papilla short, horizontally placed, cylindrical, with rounded tip; it is shorter than

753    male atrium (Fig. 13A-C). Male atrium as long as 1.2 its height, with smooth folds. A large,

754    transverse, annular fold strongly narrows communication with female atrium (Fig. 13A, C).

755    Penis papilla and male atrium clothed with a cuboidal-to-columnar, non-ciliated epithelium; the

756    subapical portion of its cells is xanthophil. Papillar epithelium pierced by necks two types of

757    cells producing granules, one erythrophil, another weakly basophil. Additionally, cells with gross

758    necks (6 µm in diameter) and erythrophil amorphous appearance are located immediately under

759    the epithelium. Epithelium of penis papilla and that of male atrium underlain by a 6-µm-thick

760    layer of circular muscle fibers.

761          Ovaries ellipsoid, with 100 µm anteroposteriorly (Fig. 13D), located immediately above

762    the ventral nerve plate, at a distance from anterior tip equivalent to 21% of body length.

763    Ovovitelline ducts arise from dorso-external side of ovaries, subsequently run backwards above

764    the ventral nerve plate. They ascend laterally to the female atrium to unite the common glandular

765    ovovitelline duct dorsally to mid female atrium (Fig. 13A). The distal half ascending portion of

766    the ducts receives shell glands. 0.9-mm-long common glandular ovovitelline duct (47% of the

767    length of female atrium) communicates with the female genital canal, this a projection of the

768    postero-dorsal portion of the female atrium directed forwards and dorsally. <u>Female atrium with</u>

769    <u>3.2x the length of male atrium.</u> Posterior third of female atrium with lateral folds narrowing its

770    lumen. Female atrium lined with a non-ciliated, 20 µm tall epithelium along anterior 3/4 of its

771    length; tissue of posterior portion is damaged. Gland cells producing erythrophil granules

772    discharge their secretion into female atrium. It seems to be underlain by two muscle layers, but

773    sections are suboptimal in quality.

774    **Remarks**

775        This small species displays a color pattern that cannot be confounded with any of its

776    congeners. Regarding the internal morphology, only *C. piguaiatui* resembles *C. imbiri* in that

777    both species have an uncommonly long female atrium, at least 2.5 times longer than the male

778    one. Indeed, *C. piguaiatui* and *C. imbiri* are very alike each other in the general aspect of the

779    copulatory apparatus. They distinguished from each other in a set of minor anatomical details:

780    (a) the pharyngeal pouch is 600 μm anterior to the prostatic vesicle (vs. practically leveled with

781    the prostatic vesicle in *C. imbiri*); (b) dorsal insertion of the pharynx is posteriorly shifted at the

782    equivalent of 20% the length of pharynx (vs. 7% in *C. imbiri*); (c) paired portion of the prostatic

783    vesicle is 1/3th of total length of this organ in *C. piguaiatui* (vs. half in *C. piguaiatui*); (d)

784    epithelium of penis papilla is underlain by a layer of circular muscle fibers followed by a layer of

785    longitudinal one in *C. piguaiatui* (vs. only a layer of circular muscle in *C. imbiri*); and (e) the

786    female atrium narrows abruptly towards its posterior section in *C. piguaiatui* (vs. gradually in *C.*

787    *imbiri*). The molecular based phylogeny shows these two species as very close genetically,

788    nonetheless, the molecular delimitation shows them to be two clearly distinct species which

789    reinforces the minor anatomical differences found to be in fact species specific.

790

791    ***Cratera paraitinga* sp. nov., Araujo, Carbayo, Riutort & Álvarez-Presas**

792    urn:lsid:zoobank.org:act:7B3F43A7-2794-42F4-B99F-B8C062F972CF

793

794    **Etymology.** The name *paraitinga* refers to São José do Paraitinga, former name of Salesópolis,

795 type locality of the species.

796 **Type locality.** Estação Biológica de Boraceia, Salesópolis, São Paulo State, Brazil.

797 **Distribution.** Type locality only.

798 **Material studied.** Holotype F5769 (MZUSP PL 2157): Estação Biológica de Boraceia,

799 Salesópolis, São Paulo State, Brazil (-23.65413, -45.88884). F. Carbayo et al., 20 April 2013.

800 Transverse sections of cephalic extremity on 19 slides; horizontal sections of a portion

801 immediately behind on 71 slides; transverse sections of pre-pharyngeal on 22 slides; sagittal

802 sections of the pharynx on 33 slides; sagittal sections of copulatory apparatus on 60 slides.

803 Paratype F5745 (MZUSP PL 2156): Ibidem. Transverse sections of cephalic extremity on 11

804 slides; horizontal sections of an immediately behind on 23 slides; transverse sections of pre-

805 pharyngeal on 7 slides; sagittal sections of pharynx and copulatory apparatus on 12 slides.

806 **Diagnosis**

807  Species of *Cratera* 76 mm long preserved; dorsal melon yellow median stripe, bordered

808 on either side by a jet black stripe external to each a marginal traffic white stripe; body margins

809 jet black; eyes marginal; anterior 1/6th of the body colored with a gradient of carmine red;

810 pharynx bell-shaped; pharyngeal pouch leveled with prostatic vesicle; distal dilatation of

811 ejaculatory duct relatively large; penis papilla as long as male atrium; female atrium 2.4 times

812 longer than the male atrium; common glandular ovovitelline duct long.

813 **Description**

814  Preserved holotype is 76 mm in length and 7 mm in width. Paratype (incompletely

815 mature), 27 and mm 4, respectively. The body is slightly lanceolate, with maximum width at the

816 level of the pharynx. Anterior to it, body thinner gradually to the rounded extremity; near

817 posterior extremity thinner more abruptly to the pointed tip. Dorsum convex, ventral side

818　flattened. Creeping sole, 95% of body width at pre-pharyngeal region. Mouth at a distance from

819　anterior extremity equal to 63% of body length; gonopore, 83% (holotype).

820　　Dorsum with an orange luminous median stripe, 40% of the body width, this bordered on

821　either side by a jet-black stripe (14.5%), external which a white band (11%); body margin (4.5%)

822　jet black (Fig. 14A-B). Body sides of anterior 1/5th of the body colored with a gradient of

823　carmine red. Ventrally, body sides of anterior 1/6th orange brown, grey white behind (Fig. 14C).

824　　Each eye is formed by a single pigmented cup with 25 μm in diameter. No clear halos

825　around eyes were seen. Eyes contour the anterior extremity in a single row and extend

826　marginally until posterior tip. Sensory pits, 15 μm deep, as a uniserial ventro-lateral row, from

827　anterior extremity through a body length at least equal to 15% of body length (holotype). Necks

828　of two types of cell glands, producing xanthophil and erythrophil granules, respectively, pierce

829　prepharyngeal region dorsally and ventrally. Besides, rhabditogen cells discharge their secretion

830　through dorsal epithelium. Conspicuous glandular margin constituted of abundant glands

831　producing xanthophil granules (Fig. 15A).

832　　Cutaneous musculature of a subepithelial circular layer, followed by two diagonals with

833　decussate fibers, and then a strongly developed longitudinal, 35-40 μm thick (paratype and

834　holotype, respectively) dorsally and 40-45 μm thick ventrally (holotype and paratype,

835　respectively). Thickness of cutaneous muscle ranges from 6.6% (holotype) to 10.7% (paratype)

836　to body height in the pre-pharyngeal region.

837　　Three parenchymal muscle layers present throughout the body, all constituted by fibers

838　relatively densely packed: a dorsal layer of diagonal decussate fibers (10 μm thick, holotype), a

839　supraintestinal layer of transverse muscle fibers (40 μm), and a transverse subintestinal one (40

840　μm). Dorso-ventral fibers abundant between intestinal branches.

841        Central nervous system as a ventral nerve plate. Clearly evident cerebral ganglia were not

842    found.

843        Mouth located in the end of the anterior half of pharyngeal pouch (Fig. 15B). Pharynx

844    bell-shaped, with dorsal insertion posterior to the ventral at the equivalent of 40% of pharyngeal

845    length. Esophagus length, 20% of pharyngeal length (holotype and paratype). Outer pharyngeal

846    epithelium underlain by a one-fiber-thick layer (4 μm) of longitudinal muscle fibers followed by

847    a layer of circular fibers (6 μm); inner pharyngeal epithelium underlain by a layer (50-100 μm)

848    of circular fibers, followed by a layer (20 μm) of longitudinal fibers (holotype). Pharyngeal

849    pouch at 80 μm from prostatic vesicle (holotype), i.e., 0.001% of body length.

850        Testes dorsal, located under the supraintestinal muscle layer, partially placed between the

851    intestinal diverticula (Fig. 15A). These testes extend from shortly behind the level of the ovaries

852    to nearly 3 mm anterior to root of pharynx (holotype). Sperm ducts communicate with the

853    respective lateral diverticulum of the prostatic vesicle. This vesicle extrabulbar, elongate, with

854    anterior 1/4th of its length branched. Vesicle runs posteriorly and upwards until anterior region

855    of penis bulb. Vesicle is lined with a ciliated epithelium, which is pierced by numerous necks of

856    cells producing fine erythrophil granules. A 15-μm-thick net of muscle fibers surround the

857    vesicle. Inside the penis papilla, vesicle communicates with a straight ejaculatory duct traversing

858    penis papilla at the tip of which dilates to a conspicuous cavity with half of penis papilla length

859    (Fig. 15C, 16A-B). Epithelium of this duct surrounded by a 5-μm-thick layer of circular muscle

860    fibers along most of its length, and of circular and longitudinal fibers in its dilated portion.

861        Penis papilla conical, with dorsal insertion slightly posterior to the ventral one; it is as

862    long as male atrium (Fig. 15C, 16A). Male atrium as long as 1.4x its height, slightly folded.

863    Penis papilla and male atrium clothed with a cuboidal, non-ciliated epithelium, which is pierced

864      by necks of cells producing erythrophil granules. Quality of stain did not provide further details.

865      Epithelium of penis papilla and that of male atrium underlain by a 3-μm-thick layer of circular

866      muscle fibers, followed by a 2-μm-thick layer of longitudinal fibers.

867         Ovaries elongated, ovoid, with 300 μm anteroposteriorly. They are located immediately

868      above the ventral nerve plate, at a distance from anterior tip equivalent to 25% of body length

869      (holotype). Ovovitelline ducts arise from dorso-lateral side of the ovaries and run backwards

870      above the ventral nerve plate. They ascend laterally to the female atrium to unite the common

871      glandular ovovitelline duct dorsally to female atrium (Fig. 15C). Distal ascending portion of the

872      ducts receives shell glands. The long common glandular ovovitelline duct (0.9 mm, ie., 1/3th of

873      the length of female atrium) communicates with female genital canal, the latter being a

874      projection of posterior portion of female atrium that runs forwards and dorsally (Fig. 15C, 16A-

875      C). Female atrium long and funnel-shaped, compressed laterally. Anterior portion of female

876      atrium narrower. Female atrium with 2.4 times the length of male atrium, and lined with non-

877      ciliated epithelium, 40 μm tall and with multilayered aspect in its posteriormost 1/4th; otherwise,

878      20 μm tall and cuboidal-to-columnar. Necks of cells producing erythrophil granules pierce

879      female epithelium, this underlain by a layer of circular muscle fibers (10 μm thick, holotype)

880      followed by a layer of longitudinal fibers (10 μm thick).

881      **Remarks**

882         Among all species of the genus, *C. taxiarcha* and *C. piguaiatui* resemble *C. paraitinga* in

883      the general color pattern of the dorsum consisting of longitudinal stripes with black, white and

884      yellow color. However, the median stripe in *C. taxiarcha* is white (vs. yellowish in *C.*

885      *paraitinga*). *Cratera piguaiatui*, very similar to *C. paraitinga* in the color pattern, differs from it

886      in the width of the yellowish midstripe (28% of body width in *C. piguaiatui* vs. 40% in *C.*

887  *paraitinga*).

888  Regarding the copulatory apparatus, only *C. piguaiatui* and *C. imbiri* resemble *C.*

889  *paraitinga* in the relatively long female atrium when compared with the male one. However, the

890  two species differ from *C. paraitinga* in minor details: (a) the dilatation of the ejaculatory duct is

891  relatively small in *C. piguaiatui* (vs. relatively large in *C. paraitinga*); (b) the pharyngeal pouch

892  is 0.6 mm anterior to the prostatic vesicle in *C. piguaiatui* (vs. practically leveled in *C.*

893  *paraitinga*); (c) the penis papilla is shorter than the male atrium in *C. piguaiatui* and *C. imbiri*

894  (vs. as long as the male atrium in *C. paraitinga*).

895  The molecular analyses show these three species, *C. piguaiatui*, *C. imbiri* and *C.*

896  *paraitinga*, to constitute a monophyletic group, which will explain their morphological

897  similitudes commented above and could also raise some doubt on their identity as different

898  species. However, the discovery methods of species delimitation, only with the exception of the

899  mPTP method, show the three as independent species. In the case of the validation method (BPP)

900  the significance of the separation of *C. imbiri* and *C. paraitinga* is only highly supported by the

901  models implying a small ancestral size, while the support is slightly lower if we consider

902  ancestral population was large. It could be interpreted from our results that ancestral populations

903  may not have been very large, although, of course, the current situation may be a consequence of

904  the destruction of their habitat or a lack of sampling, since some areas have been explored very

905  intensively and others are still pending sampling. Putting together all the evidence, molecular

906  and morphology reinforce one another and give more weight to the small morphological

907  differences found to be indicators of the different lineages having become different species.

908

909  **Discussion**

910

911          Carbayo et al. (2013) proposed the first phylogenetic framework of Geoplaninae. That

912     phylogeny was inferred from one mitochondrial region (COI) and three nuclear ones (18S, 28S

913     rDNA and EF) of 68 species, eight of them representing *Cratera* lineages (plus one immature

914     representative). At that time, only three species of *Cratera* were known (*C. crioula*, *C.*

915     *pseudovaginuloides* and *C. tamoia*). Later, three of the undescribed species considered in that

916     study were formally described (*C. cuarassu*; *C. picuia* Lago-Barcia & Carbayo, 2018, *C. arucuia*

917     Lago-Barcia & Carbayo, 2018). Two species included in the Carbayo et al (2013) phylogeny that

918     had remained morphologically unstudied, are described in the present work, namely *C.*

919     *piguaiassu* and *C. piguaiatui*.

920          In the present study, three new species (*C. imbiri*, *C. paraitinga*, *C. piguaiaboja*) are also

921     included for the first time. The phylogenetic relationships between all these 11 species have been

922     examined here through comparative analysis of six concatenated DNA regions (two

923     mitochondrial fragments and four nuclear).

924          Without taking into consideration differences in representativeness, the topology of our

925     phylogeny matches that of Carbayo et al (2013), except for the position of *C. tamoia* and *C.*

926     *crioula*. In the phylogeny from 2013, *C. tamoia* is sister of the remaining species of an in-group

927     including *C. crioula*, whereas in the present phylogeny, *C. crioula* + *C. piguaiassu* is the sister

928     clade to the remaining members of the in-group, which includes *C. tamoia*. This is a relevant

929     result, due to a difference in taxon sampling. As more species are included in the present study,

930     relationships are resolved that could not be observed in the phylogenies of 2013, with a smaller

931     representation of species of *Cratera*. Lago-Barcia & Carbayo (2018) discussed the evolution of

932     some morphological attributes within *Cratera* by analyzing them against the phylogeny of

933     Carbayo et al. (2013). They considered only the five species whose anatomy was known, namely

934    *C. arucuia, C. crioula, C. cuarassu, C. picuia,* and *C. pseudovaginuloides*. They interpreted that

935    the distal widening of the ejaculatory duct originated in the common ancestor of all *Cratera*

936    members and was secondarily lost in the last common ancestor of *C. tamoia, C. crioula,* and *C.*

937    *arucuia*. For this feature as well as other characters (roof of the male atrium pierced by necks of

938    numerous cyanophil glands; prostatic vesicle dorsally located; ==90o rotation of the penis papilla==)

939    they concluded that "diagnostic character states of the genus can be lost or modified within

940    recently evolved in-groups of *Cratera*, hence puzzling species classification" (Lago-Barcia &

941    Carbayo, 2018).

942        In the light of this new phylogenetic framework, loss of the widening of distal section of

943    the ejaculatory duct apparently evolved independently in two lineages, thus giving rise to the

944    condition is *C. crioula*, and that in *C. picuia* and *C. arucuia*. However, this new framework does

945    not invalidate the above-quoted conclusion of Lago-Barcia & Carbayo. Moreover, our data

946    corroborates their conclusion as demonstrated in the following five selected examples. (i) The

947    position of the prostatic vesicle, either internal to the penis bulb or external to it, appears to have

948    independently evolved from an external to an internal position only in *C. tamoia* and *C. picuia*.

949    An equally parsimonious interpretation would be that the internal position of the prostatic vesicle

950    would have evolved in the common ancestor of *C. tamoia* + *C. arucuia* + *C. picuia* and that this

951    condition would have reversed in *C. arucuia*. (ii) In similar vein, a penis papilla longer than the

952    male atrium may have been gained in the common ancestor of *C. piguaiaboja, C.*

953    *pseudovaginuloides, C. crioula, C. piguaiassu, C. picuia, C. arucuia* and *C. tamoia*, while this

954    condition would independently secondarily have been lost in *C. piguaiaboja* and *C. tamoia*. (iii)

955    In *C. picuia* and *C. piguaiaboja*, the dorsal surface of the male atrium is traversed by a mass of

956    necks of cells producing cyanophil granules. This situation is best explained as two independent

957    gain events. (iv) The most parsimonious explanation for the very reduced or even absence of the

958    common glandular ovovitelline duct in *C. picuia*, *C. piguaiassu* and *C. piguaiaboja* is

959    independent loss in each of these species, none of which shares a sister-group relationship.

960        In bucking this trend, the relatively long female atrium, in comparison with the male

961    atrium appears to be homologous in all members of *Cratera*. The female atrium is usually as

962    long as the male one. However, in *C. piguaiatui*, *C. imbiri*, and *C. paraitinga*, the female atrium

963    is >2.4 times longer than the male one. These three species constitute a monophyletic group and

964    most probably this character state evolved in the common ancestor of these species. These three

965    species are similar to each other, not only in this trait, but also in the traditional characteristics

966    used in the classification of Geoplaninae. For this reason, our molecular approach in the species

967    delimitation proved to be essential in their discovery as independent lineages.

968        The causes underlying the evolutionary differences between the copulatory organs in land

969    triclads remain unclear. Absence of relevant apomorphies in other related groups, such as the

970    freshwater planarian genus *Girardia* (Dugesiidae), also complicated assignment of species to the

971    genus (Sluys, Hauser & Wirth, 1997). In the case of land planarians, morphological differences

972    may be related to the fact that each species belongs to a lineage that has evolved independently

973    for a long period, as exemplified by the land planarian *Cephaloflexa bergi* (Graff, 1899)

974    (Geoplaninae), a species that originated about 7 Mya (Álvarez-Presas et al., 2017).

975        As a result of this argument, it rises that *Cratera* land planarians evolved labile features,

976    even those that diagnose the genus, such as the dilatation of the ejaculatory duct. This lability can

977    mislead a natural classification of *Cratera* and its relatives if systematics is solely based on

978    morphology.

979        An interesting aspect of land planarians is their restricted geographical distribution. Most

980    species are known from only one or a few localities (unpublished results). In the present study

981    only *Cratera piguaiatui* was found in an additional locality apart from the type locality. Even so,

982    the two localities are only 30 km apart from each other. Although sampling artifacts may

983    underlie such presumably restricted distributions (Sluys, 1999) it is also possible that they reflect

984    actual species distribution. Our data support the latter in the case of *Cratera* because we

985    performed an intensive sampling effort in the four areas that resulted in the distributional ranges

986    reported in this study.

987        We hypothesize here that *Cratera* species presenting such labile features, being

988    genetically close among them and with very restricted areas of distribution may be the result of

989    relatively recent speciation events linked to the postglacial history of the area. However,

990    thorough studies including NGS data and robust population analyses will be necessary to

991    confirm such hypothesis.

992
993
994    **Conclusions**
995

996        Molecular-based phylogenies and species delimitation provide hypotheses on species

997    recognition that are independent from the morphology-based approach. Congruence of both

998    approaches allowed us to recognize evolutionarily independent lineages, i.e, species, and to

999    independently evaluate minor morphological differences among the individuals as a signal of

1000    diagnostic attributes of a species. Otherwise, most likely we had ranked *C. piguaiatui*, *C. imbiri*

1001    and *C. paraitinga* under one nominal species.

1002        Moreover, the new molecular markers for species delimitation and phylogenetic

1003    inference developed for the first time in the present work have shown to be highly resolutive for

1004    terrestrial planarians. We have expanded the number of informative molecular markers by

1005    adding two new molecules (Tnuc813 and Nd4toCox1) as a result of the use of new generation

1006    molecular tools. This result should not be overlooked, since the availability of molecular markers

1007    has always been a limitation in the study of the systematics of these animals.

1008
1009
1010
1011
1012
1013    **Acknowledgements**
1014

1015        We are grateful to the COTEC - Instituto Florestal do Estado de São Paulo (Proc. SMA

1016    12.640/2011), Museu de Zoologia (EBBAut.020/2013) and Instituto Chico Mendes de

1017    Conservação da Biodiversidade (Proc. 32779-1; 11748-4) for licensing the field work. We also

1018    thank Celso Barbieri Junior, Cláudia Olivares, Débora Redivo, Erica Panachuk de Souza, Júlio

1019    Pedroni, Leonardo Zerbone, Marcos Santos Silva, Marília Jucá and Welton Araújo (EACH,

1020    USP) for assistance during the sampling. Thanks are due to Geison Castro da Silveira, Lucas

1021    Beltrami, and Ítalo Silva de Oliveira Souza (EACH, USP) for histological processing. Gema

1022    Blasco is thanked for the wet lab support.

1023
1024
1025
1026
1027
1028    **References**
1029

1030    **Almeida AL, Marques FPL, Carbayo F. 2019**. Endless forms most beautiful': taxonomic

1031    revision of the planarian *Geoplana vaginuloides* (Darwin, 1844) and discovery of numerous

1032    congeners (Platyhelminthes: Tricladida). *Zoological Journal of the Linnean Society* 185: 1–65.

1033    https://doi.org/10.1093/zoolinnean/zly022

1034    **Álvarez-Presas M, Baguñà J, Riutort M. 2008**. Molecular phylogeny of land and freshwater

1035    planarians (Tricladida, Platyhelminthes): from freshwater to land and back. *Molecular*

1036    *Phylogenetics and Evolution* 47: 555–568. https://doi.org/10.1016/j.ympev.2008.01.032

1037    **Álvarez-Presas M, Carbayo F, Rozas J, Riutort M. 2011**. Land planarians (Platyhelminthes)

1038    as a model organism for fine-scale phylogeographic studies: understanding patterns of

1039    biodiversity in the Brazilian Atlantic Forest hotspot. *Journal of Evolutionary Biology* 24: 887–

1040    896. https://doi.org/10.1111/j.1420-9101.2010.02220.x

1041    **Ayres DL, Darling A, Zwickl DJ, Beerli P, Holder MT, Lewis PO, et al. 2012**. BEAGLE: An

1042    application programming interface and high-performance computing library for statistical

1043    phylogenetics. *Systematic Biology* 61: 170–173. https://doi.org/10.1093/sysbio/syr100

1044    **Bouckaert R, Heled J, Kühnert D, Vaughan T, Wu C-H, Xie D, et al. 2014**. BEAST2: A

1045    software platform for Bayesian evolutionary analysis. *PLOS Computational Biology.*

1046    https://doi.org/10.1371/journal.pcbi.1003537

1047    **Carbayo F, Álvarez-Presas M, Olivares CT, Marques FPL, Froehlich EM, Riutort M.**

1048    **2013**. Molecular phylogeny of Geoplaninae (Platyhelminthes) challenges current classification:

1049    proposal of taxonomic actions. *Zoologica Scripta* 42: 508–528.

1050    https://doi.org/10.1111/zsc.12019

1051    **Carbayo F, & Almeida AL. 2015**. Anatomical deviation of male organs of land planarians from

1052    Rio de Janeiro, Brazil, with description of two new species of *Cratera* (Platyhelminthes,

1053    Tricladida). *Zootaxa* 3931(1): 027-040. https://doi.org/10.11646/zootaxa.3931.1.2

1054 **Carbayo F, Silva MS, Riutort M, Álvarez-Presas M. 2018**. Rolling into the deep of the land

1055 planarian genus *Choeradoplana* (Tricladida, Continenticola, Geoplanidae) taxonomy. *Organisms*

1056 *Diversity & Evolution* 18: 187– 210. https://doi.org/10.1007/s13127-017-0352-4

1057 **Carranza S, Giribet G, Ribera C, Baguñà J, Riutort M. 1996**. Evidence that Two Types of

1058 18s rDNA Coexist in the Genome of *Dugesia* (*Schmidtea*) *mediterranea* (Platyhelminthes,

1059 Turbellaria, Tricladida). *Molecular Biology and Evolution* 13: 824–832.

1060 https://doi.org/10.1093/oxfordjournals.molbev.a025643

1061 **Cason. 1950**. A rapid one-step Mallory-Heidenhain stain for connective tissue. *Stain Technology*

1062 25(4): 225–226. https://doi.org/10.3109/10520295009110996

1063 **Darriba D, Taboada GL, Doallo R, Posada D. 2012**. jModelTest 2: more models, new

1064 heuristics and parallel computing. *Nature Methods* 9: 772. https://doi.org/10.1038/nmeth.2109

1065 **Froehlich EM. 1955**. Sobre espécies brasileiras do gênero *Geoplana*. *Boletim da Faculdade de*

1066 *Filosofia, Ciências e Letras da Universidade de São Paulo, Série Zoologia* 19: 289–369.

1067 **Hall TA. 1999**. BioEdit: a user-friendly biological sequence alignment editor and analysis

1068 program for Windows 95/98/NT. *Nucleic acids symposium series* 41: 95–98.

1069 **Kapli P, Lutteropp S, Zhang J, Kobert K, Pavlidis P, Stamatakis A, et al. 2017**. Multi-rate

1070 Poisson tree processes for single-locus species delimitation under maximum likelihood and

1071 Markov chain Monte Carlo. *Bioinformatics* 33: 1630–1638.

1072 https://doi.org/10.1093/bioinformatics/btx025

1073 **Katoh K, Rozewicki J, Yamada KD. 2017**. MAFFT online service: multiple sequence

1074 alignment, interactive sequence choice and visualization. *Briefings in Bioinformatics bbx108:* 1–

1075 7. https://doi.org/10.1093/bib/bbx108

1076 **Lago-Barcia D & Carbayo F. 2018**. Taxonomic revision of four species of the Neotropical land

1077 planarian genera *Cratera* and *Geoplana* (Platyhelminthes, Tricladida) with a description of two

1078 new species and an emendation of *Cratera*. *Zootaxa* 4500 (4): 517–542.

1079 https://doi.org/10.11646/zootaxa.4500.4.3

1080 **Lanfear R, Frandsen PB, Wright AM, Senfeld T, Calcott B. 2017**. Partitionfinder 2: New

1081 methods for selecting partitioned models of evolution for molecular and morphological

1082 phylogenetic analyses. *Molecular Biology and Evolution* 34: 772–773.

1083 https://doi.org/10.1093/molbev/msw260

1084 **Lázaro EM, Sluys R, Pala M, Stocchino GA, Baguñà J, Riutort M. 2009**. Molecular

1085 barcoding and phylogeography of sexual and asexual freshwater planarians of the genus *Dugesia*

1086 in the Western Mediterranean (Platyhelminthes, Tricladida, Dugesiidae). *Molecular*

1087 *Phylogenetics and Evolution* 52: 835–845. https://doi.org/10.1016/j.ympev.2009.04.022

1088 **Leria L, Vila-Farré M, Álvarez-Presas M, Sánchez-Gracia A, Rozas J, Sluys R, Riutort M.**

1089 **2020**. Cryptic species delineation in freshwater planarians of the genus *Dugesia*

1090 (Platyhelminthes, Tricladida): Extreme intraindividual genetic diversity, morphological stasis,

1091 and karyological variability. *Molecular Phylogenetics and Evolution*, 143: 106496.

1092 https://doi.org/10.1016/j.ympev.2019.05.010

1093 **Marcus E. 1951**. Turbellaria brasileiros (9). *Boletim da Faculdade de Filosofia, Ciências e*

1094 *Letras da Universidade de São Paulo, Série Zoologia* 16: 1–217.

1095 **Miller MA, Pfeiffer W, Schwartz T. 2010**. Creating the CIPRES Science Gateway for

1096 Inference of Large Phylogenetic Trees. *Proceedings of the Gateway Computing Environments*

1097 *Workshop (GCE)*. New Orleans, LA; 1–8. https://doi.org/10.1109/GCE.2010.5676129

1098 **Minh BQ, Nguyen MAT, Von Haeseler A. 2013**. Ultrafast approximation for phylogenetic

1099 bootstrap. *Molecular Biology and Evolution* 30: 1188–1195.

1100 https://doi.org/10.1093/molbev/mst024

1101 **Negrete L, & Brusa F. 2016**. First report of the genus Cratera (Platyhelminthes, Geoplanidae) in

1102 Argentina, with description of a new species and comments on the species of the genus. *ZooKeys*

1103 610: 1–12. https://doi.org/10.3897/zookeys.610.9465

1104 **Nguyen LT, Schmidt HA, Von Haeseler A, Minh BQ. 2015**. IQ-TREE: A fast and effective

1105 stochastic algorithm for estimating maximum-likelihood phylogenies. *Molecular Biology and*

1106 *Evolution* 32: 268–274. https://doi.org/10.1093/molbev/msu300

1107 **Puillandre N, Modica MV, Zhang Y, Sirovich L, Boisselier MC, Cruaud C, et al. 2012a**.

1108 Large-scale species delimitation method for hyperdiverse groups. *Molecular Ecology* 21: 2671–

1109 2691. https://doi.org/10.1111/j.1365-294X.2012.05559.x

1110 **Puillandre N, Lambert A, Brouillet S, Achaz G. 2012b**. ABGD, Automatic Barcode Gap

1111 Discovery for primary species delimitation. *Molecular Ecology* 21: 1864–1877.

1112 https://doi.org/10.1111/j.1365-294X.2011.05239.x

1113 **Ronquist F, Teslenko M, Van Der Mark P, Ayres DL, Darling A, Höhna S, et al. 2012**.

1114 MrBayes 3.2: Efficient Bayesian Phylogenetic Inference and Model Choice Across a Large

1115 Model Space. *Systematic Biology* 61: 539–542. https://doi.org/10.1093/sysbio/sys029

1116 **Riester A. 1938**. Beiträge zur Geoplaniden-Fauna Brasiliens. *Abhandlungen der*

1117 *Senckenbergischen Naturforschenden Gesellschaft* 441: 1–88.

1118 **Rossi I, Amaral SV, Ribeiro GG, Cauduro GP, Fick I, Valiati VH, Leal-Zanchet AM. 2016**.

1119 Two new Geoplaninae species (Platyhelminthes: Continenticola) from Southern Brazil based on

1120 an integrative taxonomic approach. *Journal of Natural History* 50(13-14): 787-815.

1121 https://doi.org/10.1080/00222933.2015.1084057

1122 **Rossi I & Leal-Zanchet A. 2017**. Three new species of *Cratera* Carbayo et al., 2013 from

1123 *Araucaria* forests with a key to species of the genus (Platyhelminthes, Continenticola). *ZooKeys*

1124 643: 1–32. https://doi.org/10.3897/zookeys.643.11093

1125 **Sluys R, Hauser J, Wirth QJ. 1997**. Deviation from the Groundplan: a unique new species of

1126 freshwater planarian from South Brazil (Platyhelminthes, Tridadida, Paludicola). *Journal of*

1127 *Zoology* 241(3): 593-601. https://doi.org/10.1111/j.1469-7998.1997.tb04851.x

1128 **Sluys R. 1999**. Global diversity of land planarians (Platyhelminthes, Tricladida, Terricola): a

1129 new indicator-taxon in biodiversity and conservation studies. *Biodiversity & Conservation* 8(12):

1130 1663-1681. https://doi.org/10.1023/A:1008994925673

1131 **Sluys R, Mateos E, Riutort M, Alvarez-Presas M. 2016**. Towards a comprehensive,

1132 integrative analysis of the diversity of European microplaninid land flatworms (Platyhelminthes,

1133 Tricladida, Microplaninae), with the description of two peculiar new species. *Systematics and*

1134 *Biodiversity* 14(1): 9-31. https://doi.org/10.1080/14772000.2015.1103323

1135 **Sluys R. 2016**. Invasion of the flatworms. *American Scientist* 104(5): 288-295.

1136 https://doi.org/10.1511/2016.122.288

1137 **Talavera G & Castresana J. 2007**. Improvement of Phylogenies after Removing Divergent and

1138 Ambiguously Aligned Blocks from Protein Sequence Alignments. *Systematic Biology* 56: 564–

1139 577. https://doi.org/10.1080/10635150701472164

1140 **Yang Z & Rannala B. 2010**. Bayesian species delimitation using multilocus sequence data.

1141 *Proceedings of the National Academy of Sciences* 107: 9264–9269.

1142 https://doi.org/10.1073/pnas.0913022107

1143    **Yang Z & Rannala B. 2014**. Unguided species delimitation using DNA sequence data from

1144    multiple loci. *Molecular Biology and Evolution* 31: 3125–3135.

1145    https://doi.org/10.1093/molbev/msu279

1146    **Yang Z. 2015**. The BPP program for species tree estimation and species delimitation. *Current*

1147    *Zoology* 61: 854–865. https://doi.org/10.1093/czoolo/61.5.854

# Figure 1

Map showing the sampling sites.

Records of the five species of *Cratera* described in this paper.
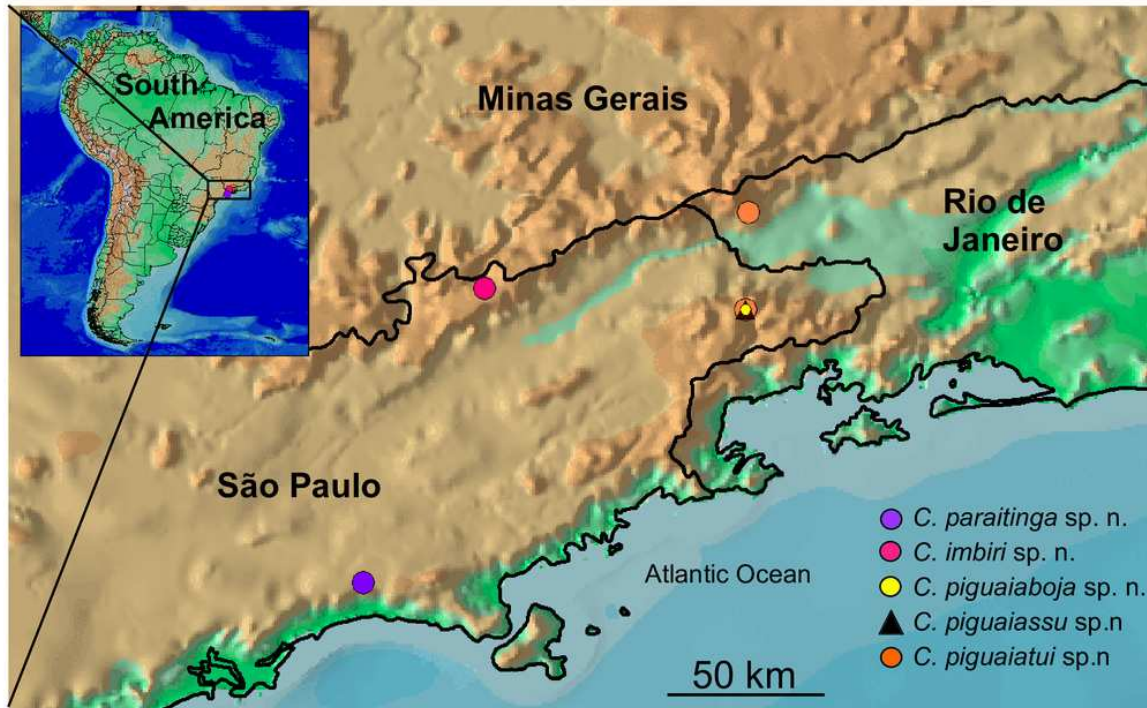
Figure 1

# Figure 2

Phylogenetic tree showing the molecular results.

Phylogenetic tree showing the topology obtained by Bayesian Inference with the information of the concatenated six genes (18S rDNA + COI + 28S rDNA + Tnuc813 + EF + Nd4toCox1). Numbers at the nodes correspond to bootstrap values of the maximum likelihood analysis (left) and those of Bayesian posterior probability (to the right). Correspondence with the PSH assigned by the molecular species delimitation methods is indicated at the nodes. Vertical bars to the right of the phylogeny show the summary of the species delimitation analyses by ABGD (purple), mPTP (yellow), BPP (green), and morphological (orange) approaches. Scale bar represents substitutions per site.
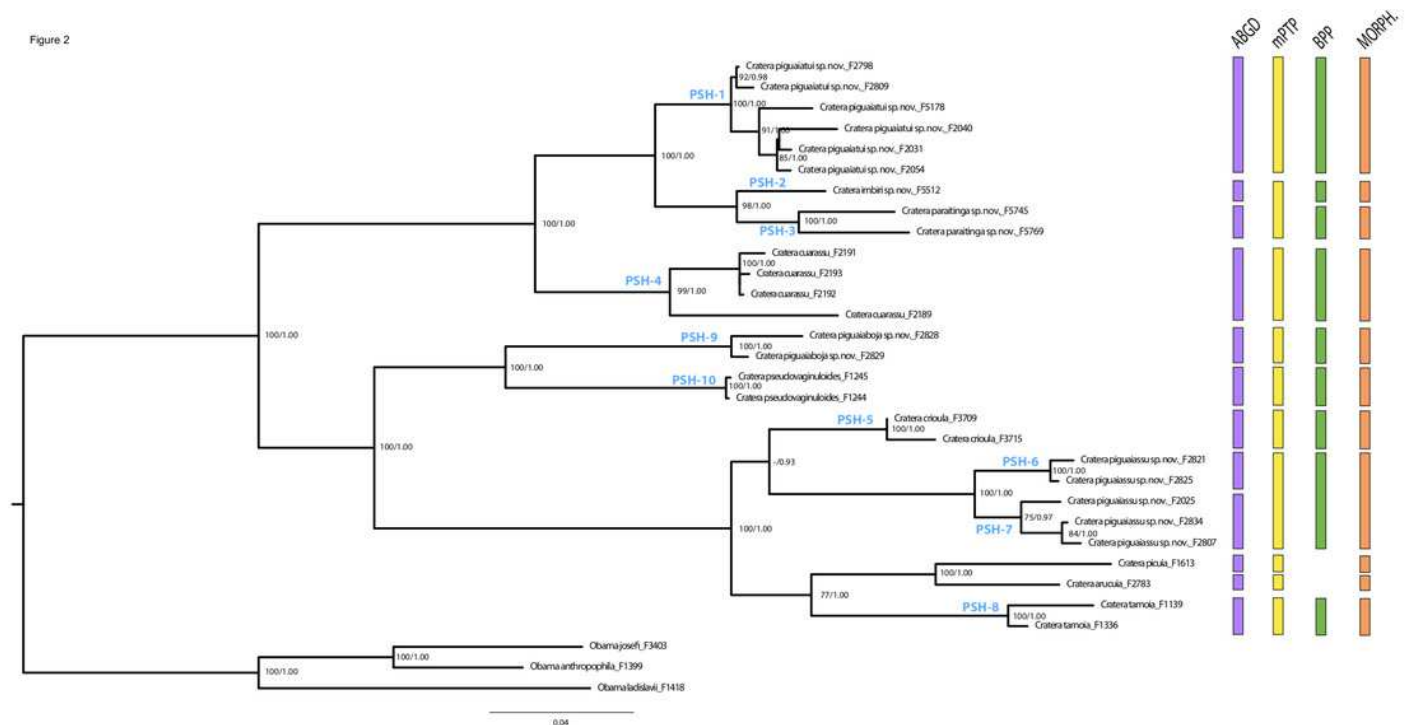
# Figure 3

Results of BPP molecular species delimitation.

Results of BPP represented in the species tree estimated with *BEAST for the genus *Cratera*. Colored squares of the nodes represent PP values for each of the applied models (M1, left up, M2, right up, M3, left down, M4, right down). Colors correspond to PP values: 1 (blue), > 0.95 (orange), or <0.95 (green). Nomenclature of Primary Species Hypothesis (PSH) is shown at the terminals of the branches. On the right, green letters indicate the Secondary Species Hypothesis validated by BPP. The images correspond to the new species. The scale bar represents substitutions per site.
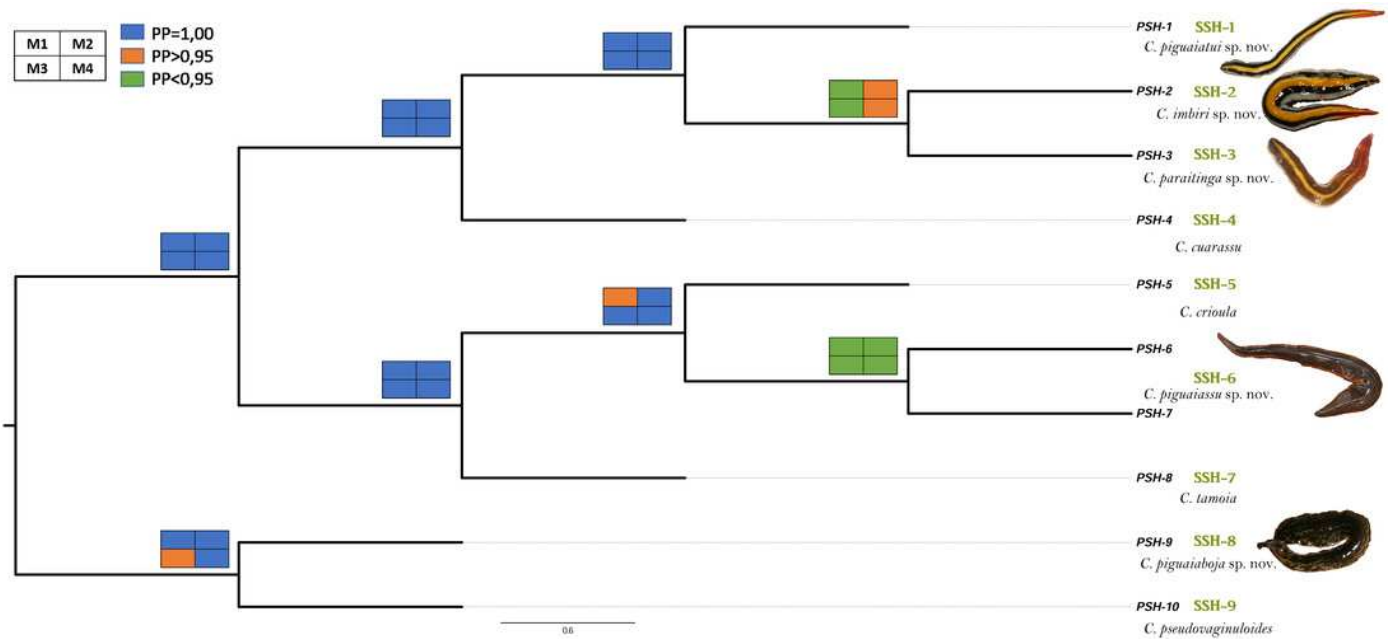
# Figure 4

*Cratera piguaiassu* sp. n. morphological characters.

*Cratera piguaiassu* sp. n. (A): dorsal and ventral (inset) views of living paratype F2807. Scale bar not available. (B): dorsal and ventral (inset) views of living paratype F2821. Scale bar not available. (C): photomicrograph of a sagittal section of the pharynx of holotype. (D): photomicrograph of a transverse section of pre-pharyngeal region of paratype F2807.
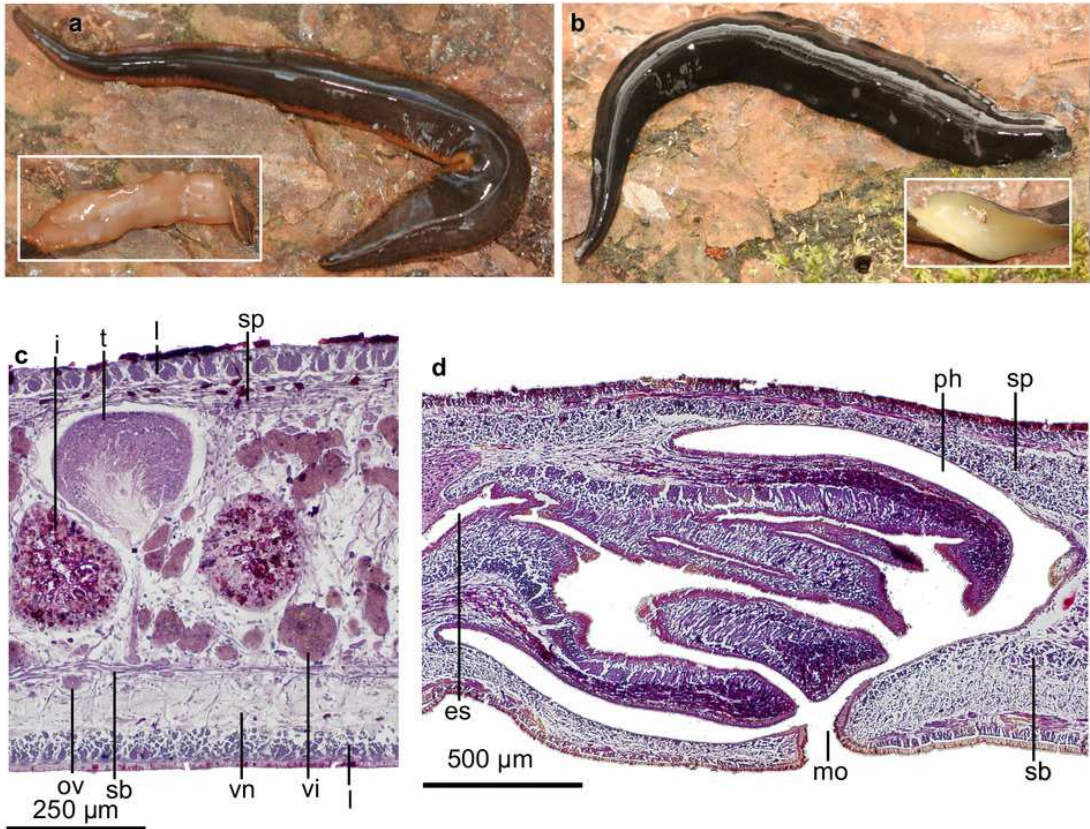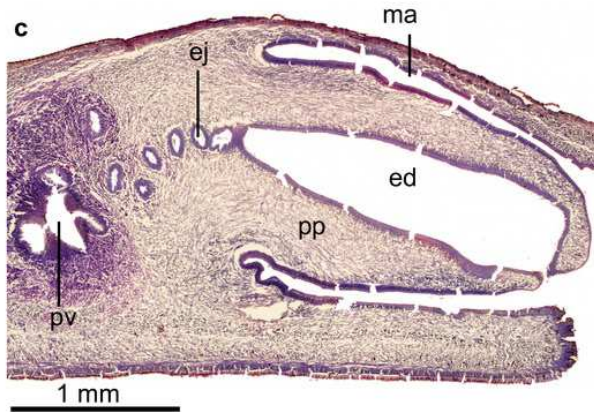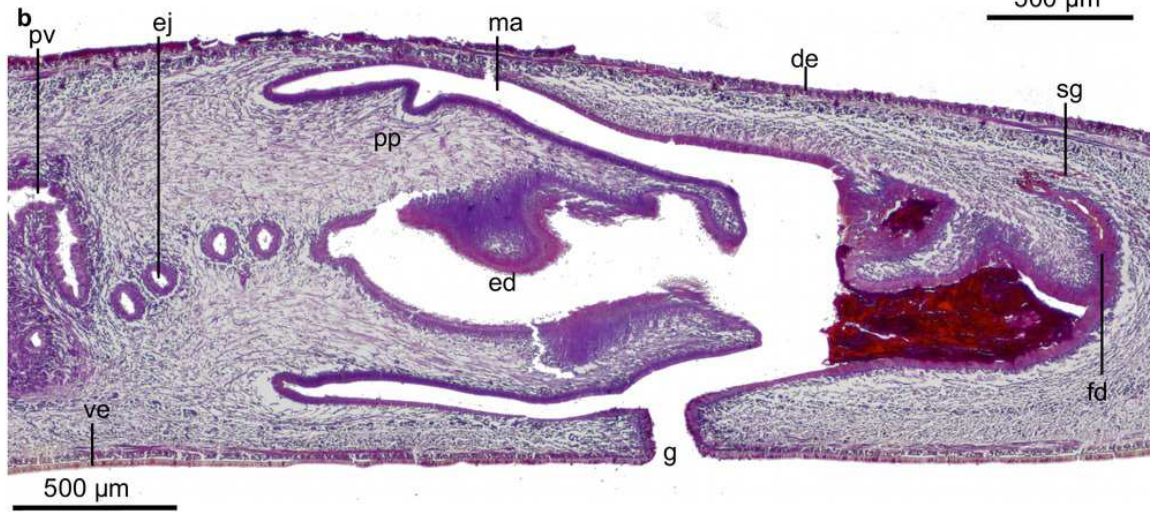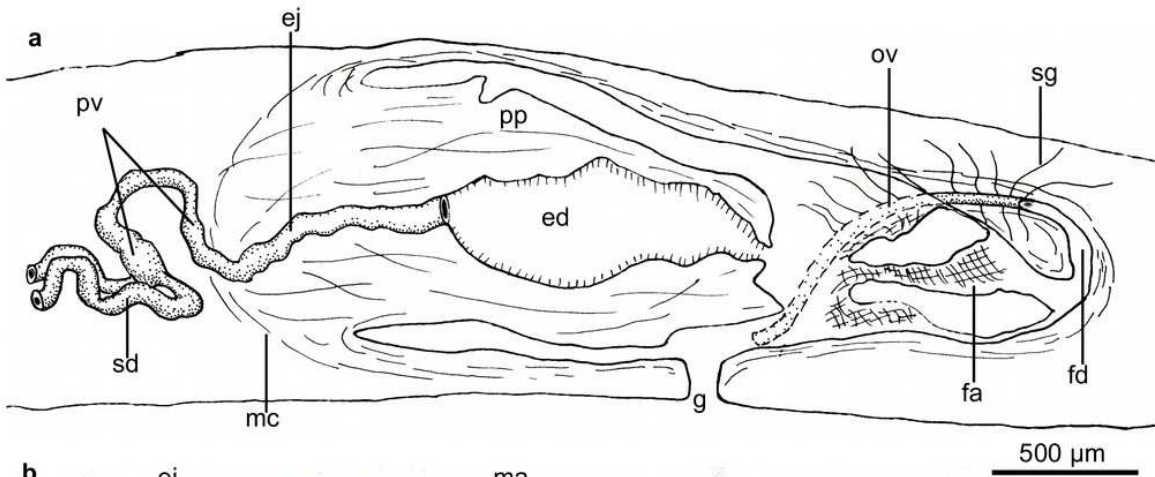
# Figure 5

*Cratera piguaiassu* sp. n. morphological details.

*Cratera piguaiassu* sp. n. (A): diagrammatic representation of the copulatory apparatus of holotype from sagittal sections. (B) photomicrograph of a sagittal section of the copulatory apparatus of holotype. (C): photomicrograph of a sagittal section of the copulatory apparatus of paratype F2821. (D): photomicrograph of a sagittal section of the female atrium of paratype F2025.
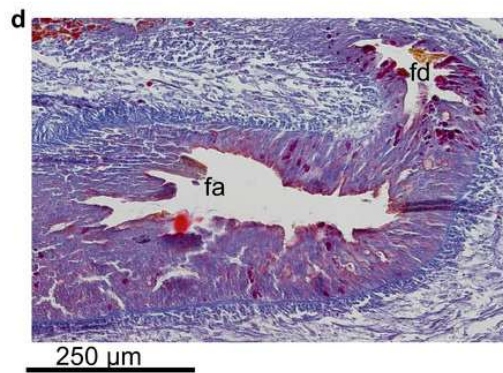
# Figure 6

*Cratera piguaiaboja* sp. n. morphological details.

*Cratera piguaiaboja* sp. n. (A): Living holotype. Scale bar not available. (B): Dorsal view of living paratype. Scale bar not available. (C): dorsal view of holotype preserved on millimeter graph paper after cutting off a piece of the body. (D): dorsal view of the paratype, preserved on millimeter graph paper after cutting off anterior extremity of the body.
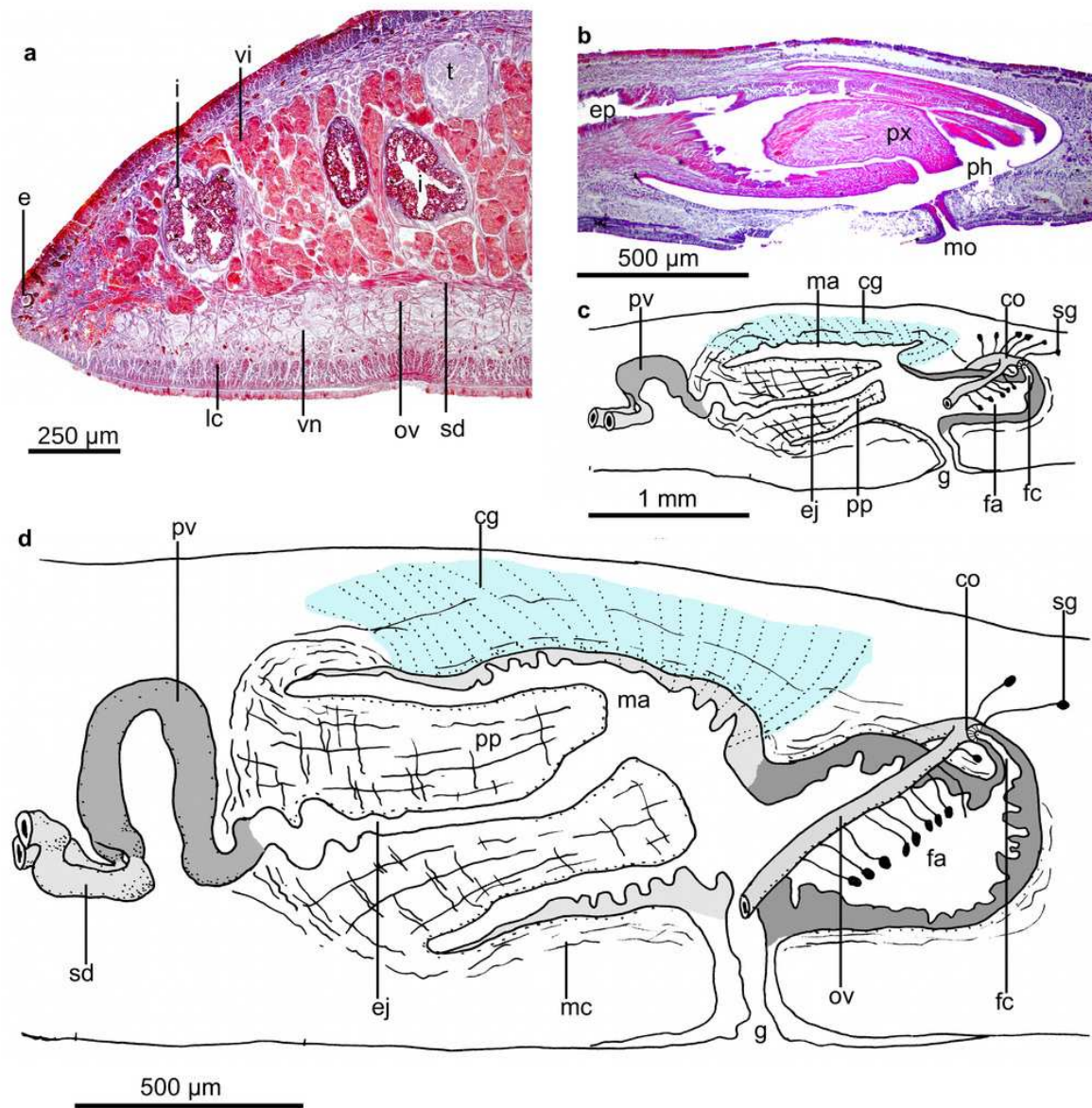
# Figure 7

*Cratera piguaiaboja* sp. n. morphological details.

*Cratera piguaiaboja* sp. n. (A): photomicrograph of a transverse section of pre-pharyngeal region of holotype. (B): photomicrograph of a sagittal section of the pharynx of paratype. (C): diagrammatic representation of the copulatory apparatus of paratype from sagittal sections. (D): diagrammatic representation of the copulatory apparatus of holotype from sagittal sections.
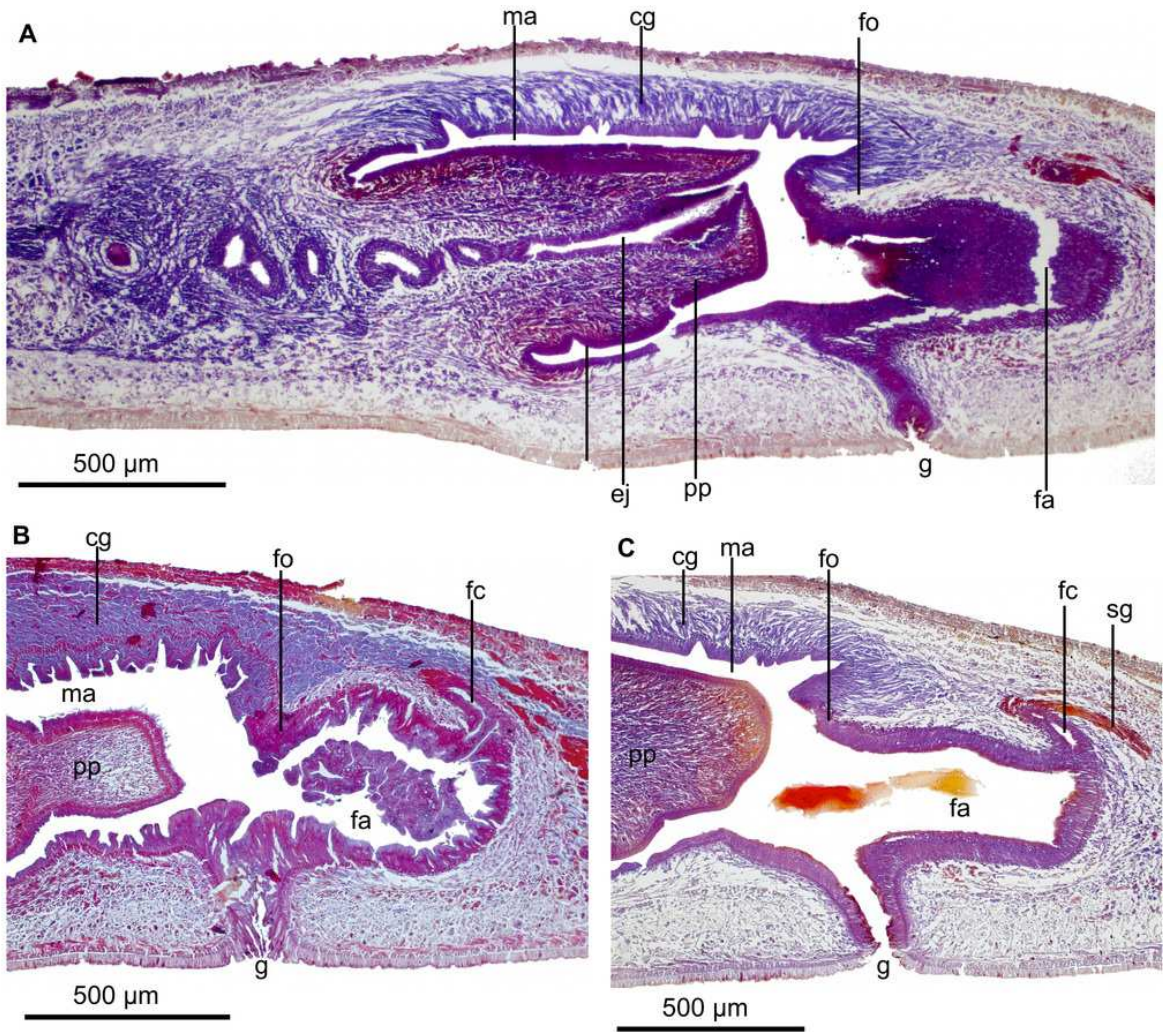
# Figure 8

*Cratera piguaiaboja* sp. n. morphological features.

*Cratera piguaiaboja* sp. n. Photomicrographs of sagittal sections. (A): Copulatory apparatus of paratype. (B): Female atrium of holotype. (C): Female atrium of paratype.

# Figure 9

Cratera piguaiatui sp. n. morphological features.

*Cratera piguaiatui* sp. n. (A): Dorsal view of living paratype F5178. (B): Dorsal view of living holotype partially twisted. Scales not available.
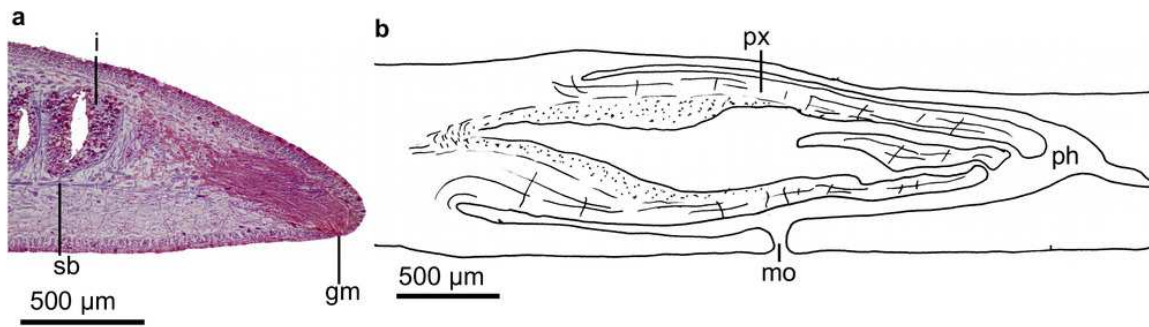
Fig. 1

# Figure 10

*Cratera piguaiatui* sp. n. morphological features.

*Cratera piguaiatui* sp. n. (A): photomicrograph of a transverse section of pre-pharyngeal region of holotype. (B): diagrammatic representation of the pharynx of paratype F2054 from sagittal sections.
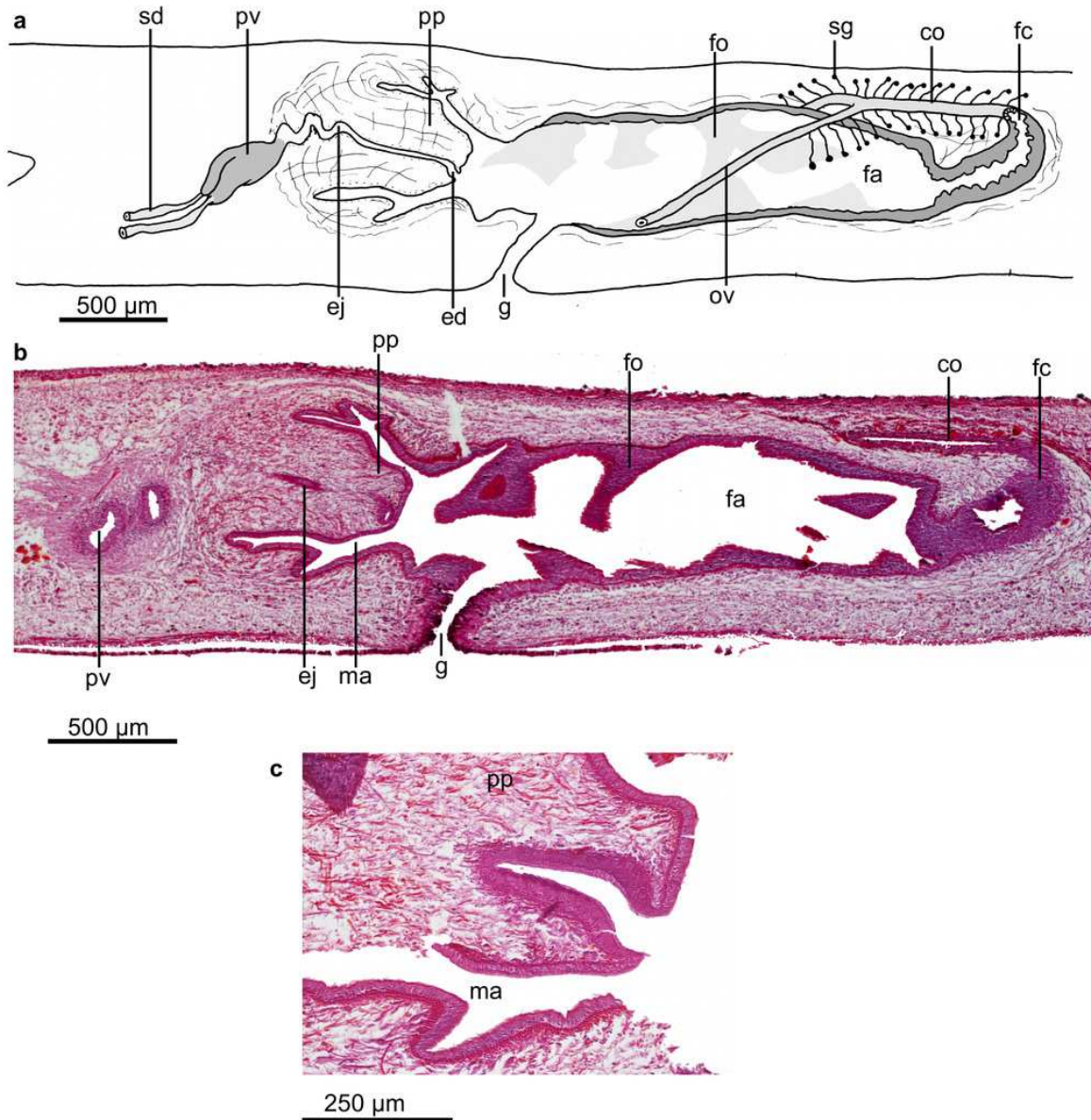
# Figure 11

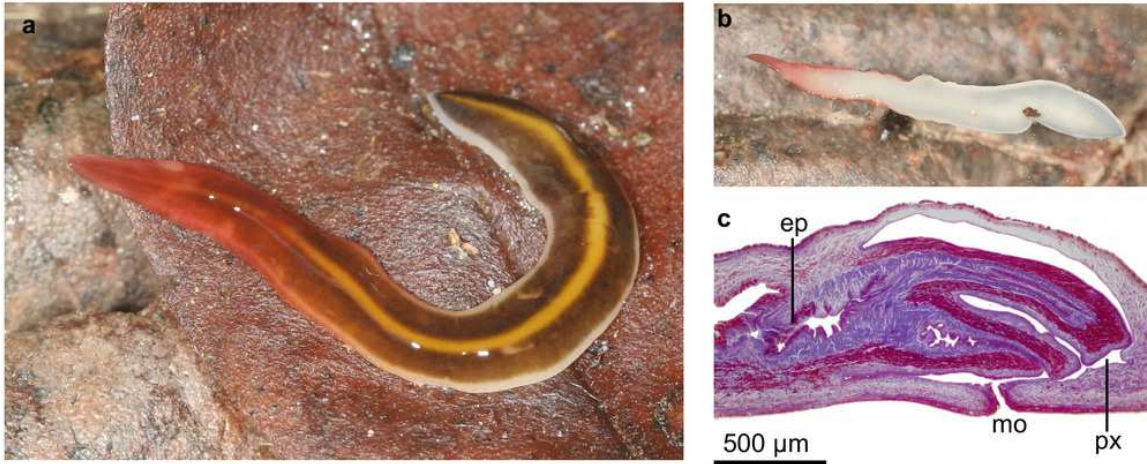*Cratera piguaiatui* sp. n. morphological details.

*Cratera piguaiatui* sp. n. Holotype. (A) diagrammatic representation of the copulatory apparatus from sagittal sections. (B): photomicrograph of a sagittal section of copulatory apparatus. (C): photomicrograph of a sagittal section penis papilla.

# Figure 12

*Cratera imbiri* sp. n. morphological features.

*Cratera imbiri* sp. n. Holotype (A): Dorsal view of living specimen. Scale bar not available. (B): Ventral view of living specimen. Scale bar not available. (C): photomicrograph of a sagittal section of pharynx.
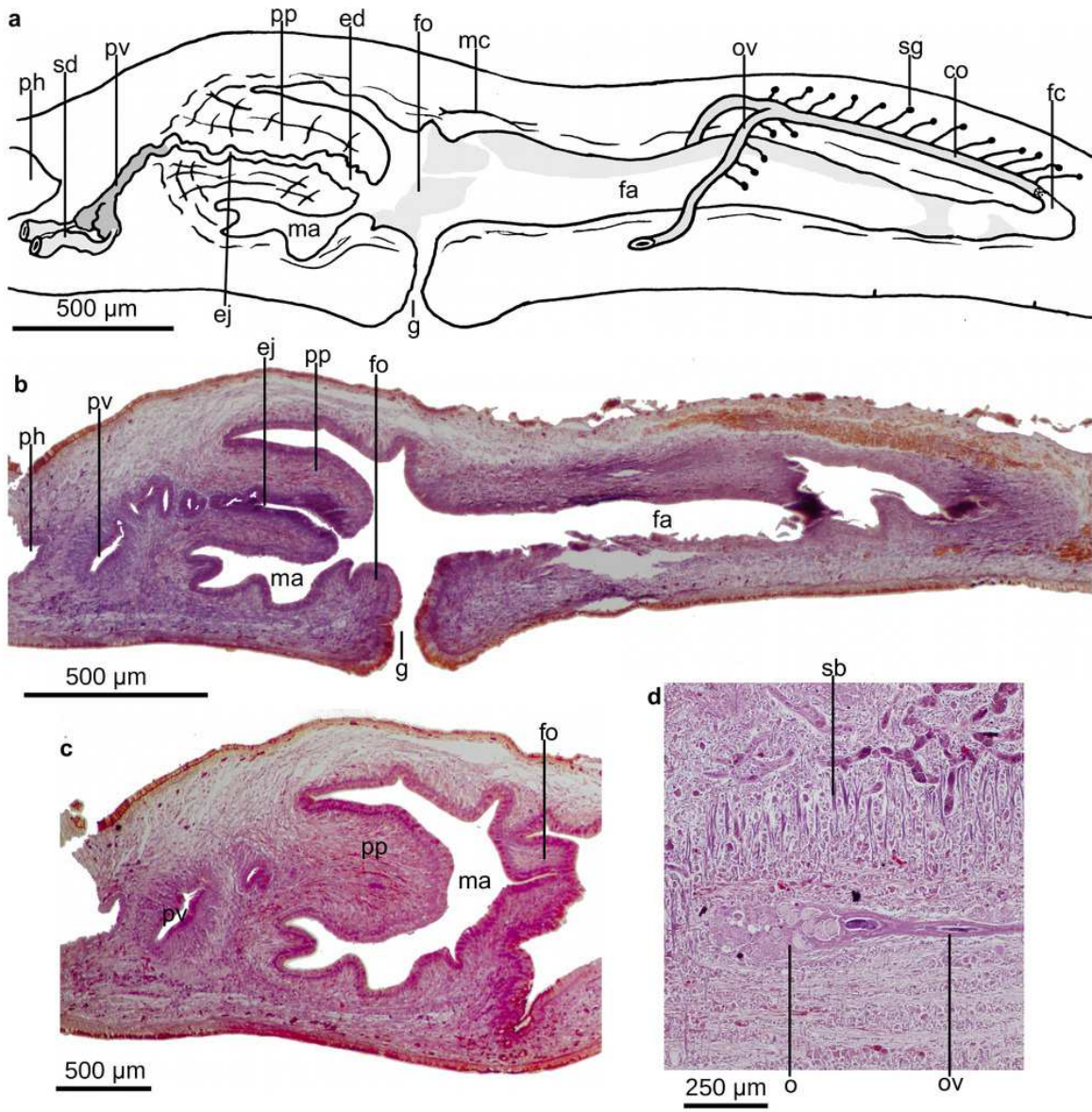
# Figure 13

*Cratera imbiri* sp. n. morphological features.

*Cratera imbiri* sp. n. Holotype. (A) diagrammatic representation of the copulatory apparatus from sagittal sections. (B): photomicrograph of a sagittal section of copulatory apparatus. (C): photomicrograph of a sagittal section of male atrium. (D): photomicrograph of a horizontal section of ovary.

# Figure 14

*Cratera paraitinga* sp. n. morphological features.

*Cratera paraitinga* sp. n. (A): Dorsal view of living holotype. (B): Dorsal view of living paratype. (C): Ventral view of living paratype. Scales not available.
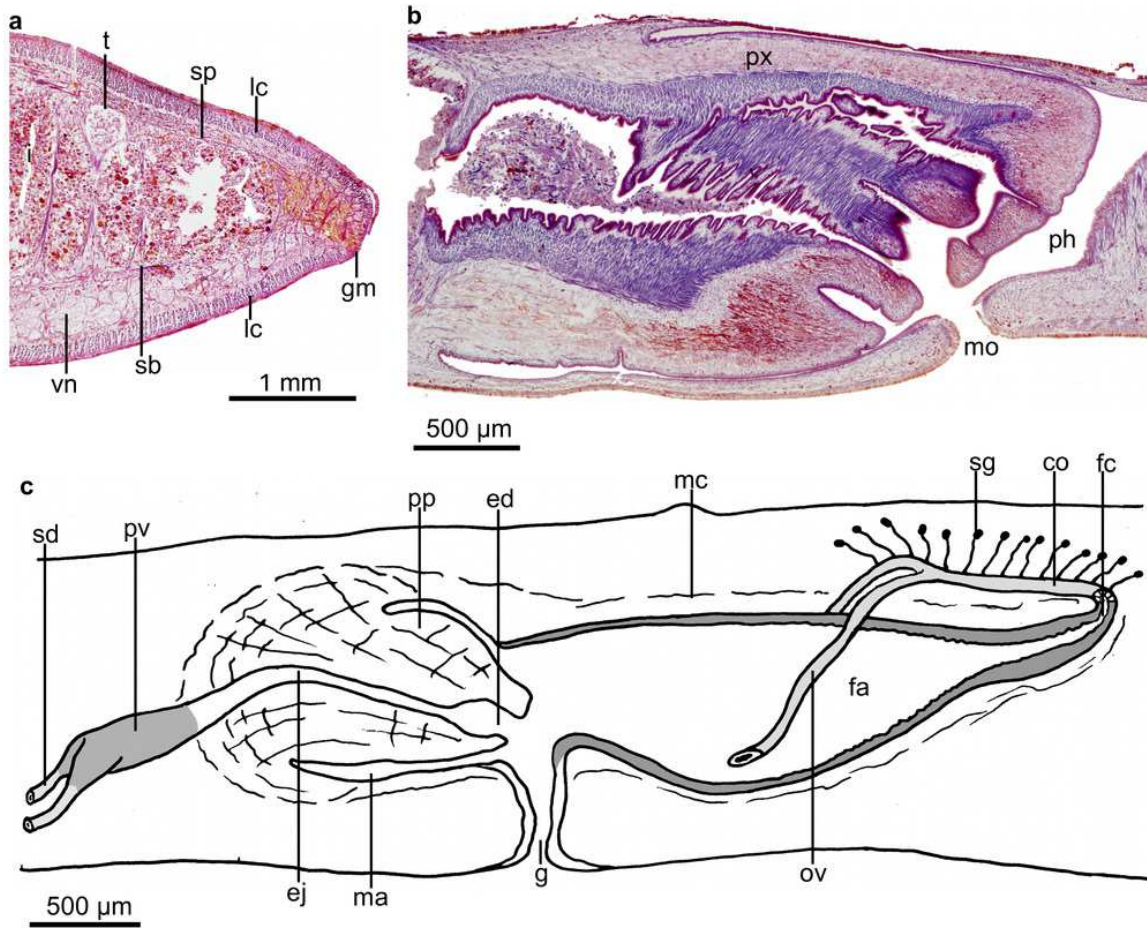
# Figure 15

*Cratera paraitinga* sp. n. morphological characters.

*Cratera paraitinga* sp. n. (A): photomicrograph of a transverse section of pre-pharyngeal region of paratype. (B): photomicrograph of a sagittal section of pharynx of holotype. (C): diagrammatic representation of the copulatory apparatus of holotype from sagittal sections.

# Figure 16

*Cratera paraitinga* sp. n. morphological features.

*Cratera paraitinga* sp. n. Photomicrographs of sagittal sections. (A): sagittal section of copulatory apparatus of holotype. (B): Copulatory apparatus of paratype, incompletely mature. (C): Posterior region of female atrium of holotype.
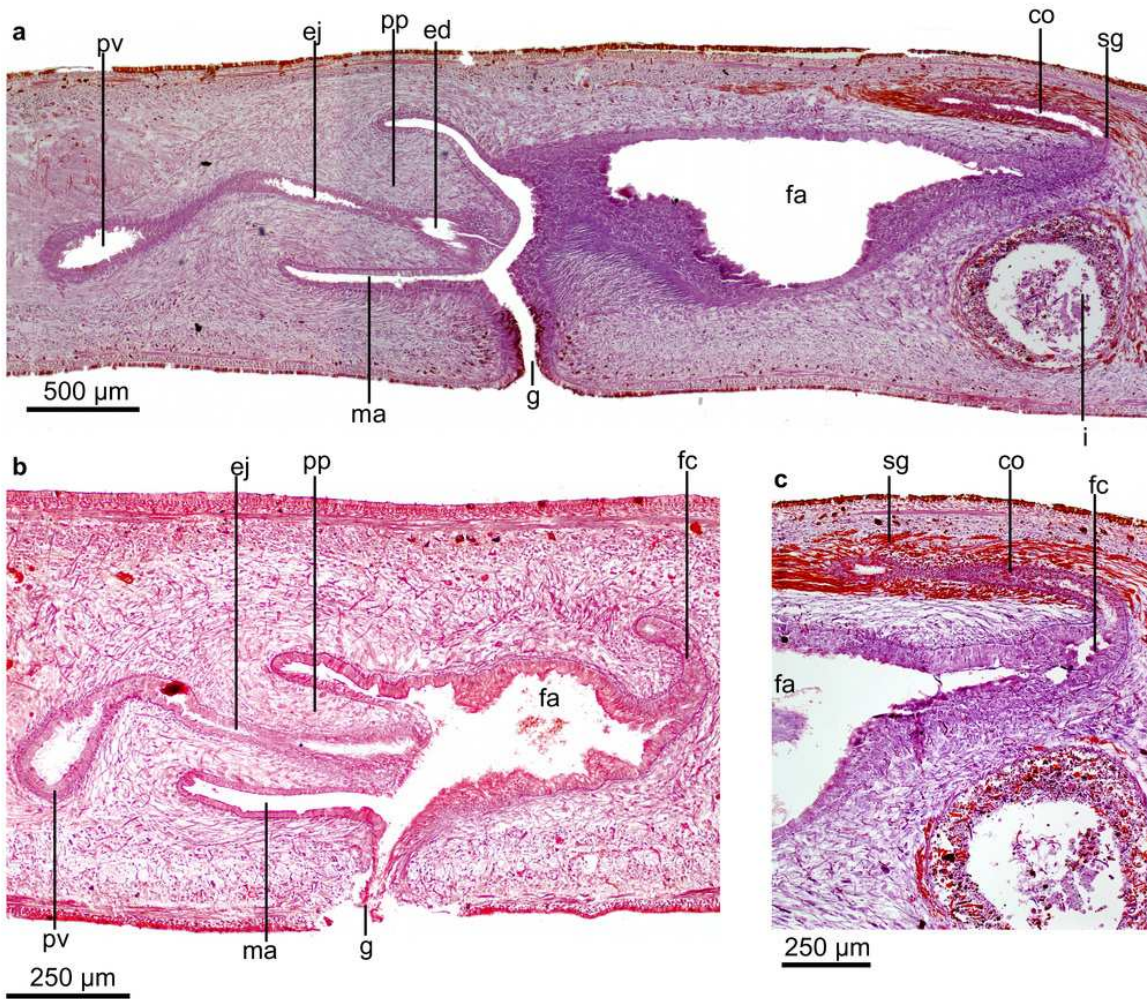
**Table 1**(on next page)

List of *Cratera* samples used in this study with sampling locality, molecular code, voucher code and GenBank Accession numbers.

1 **Table 1**. List of *Cratera* samples used in this study with sampling locality, molecular code, voucher code and GenBank Accession numbers.

| Species | Sampling locality | Molecular code | Museum Code | GenBank Accession number | | | | | |
|---|---|---|---|---|---|---|---|---|---|
| | | | | Cox1 | Nd4Cox1 | 18S | 28S | EF | Tnuc813 |
| *Cratera arucuia* | P.N. Intervales / SP | F2783 | MZUSP[a] PL 1048 | KC608281[c] | MT468629* | KC608513 | KC608396 | KC614508 | MT468607 |
| *Cratera crioula* | P.E. Serra da Cantareira / SP | F2960 | MZUSP PL 471 | MT437776* | - | - | - | - | - |
| | P.N. Bocaina / SP | F2989 | MZUSP PL 0459 | KU564215 | - | - | - | - | - |
| | P.E. Serra da Cantareira / SP | F3709 | MZUSP PL 1078 | KC608323 | - | KC608557 | KC608440 | KC614543 | MT468615 |
| | | F3715 | MZUSP PL 1079 | KC608324 | - | KC608558 | KC608441 | KC614544 | MT468616 |
| *Cratera cuarassu* | P.E. do Desengano / RJ | F2189 | MZUSP PL 348 | MT437766* | MT468626* | KC608510 | KC608393 | KC614505 | MT468603 |
| | | F2191 | MZUSP PL 349 | MT437767* | MT468627* | MT441688* | MT441711* | MT468580* | MT468604 |
| | | F2192 | MZUSP PL 350 | MT437768* | - | MT441689* | MT441712* | MT468581* | MT468605 |
| | | F2193 | MZUSP PL 351 | MT437769* | MT468628* | MT441690* | MT441713* | MT468582* | MT468606 |
| | | F4006 | MZUSP PL 805 | MT437777* | - | - | - | - | - |
| | | F4014 | MZUSP PL 806 | MT437778* | - | - | - | - | - |
| | P.E. do Desengano / RJ | F4017 | MZUSP PL 807 | MT437779* | - | - | - | - | - |
| | | F4041 | MZUSP PL 808 | MT437780* | - | - | - | - | - |
| *Cratera imbiri* sp. nov. | P.E. Campos de Jordão / SP | F5512 | MZUSP PL 2155 | MT437782* | - | MT441697* | MT441720* | MT468589* | MT468618 |
| *Cratera ochra* | | | MZU PL.00192 | KT250624[c] | - | - | - | - | - |
| | | | MZU PL.00191 | KT250623 | - | - | - | - | - |
| | | | MZU PL. 1564 | KT250622 | - | - | - | - | - |
| *Cratera paraitinga* sp. nov. | Estação Bio. Boracéia /SP | F5745 | MZUSP PL 2156 | MT437783*[c] | MT468634* | MT441698* | MT441721* | MT468590* | MT468619 |
| | | F5769 | MZUSP PL 2157 | MT437784*[c] | MT468635* | MT441699* | MT441722* | MT468591* | MT468620 |

| Species | Sampling locality | Molecular code | Museum Code | Cox1 | Nd4Cox1 | 18S | 28S | EF | Tnuc813 |
|---|---|---|---|---|---|---|---|---|---|
| *Cratera picuia* | P.N. Saint Hilaire / PR | F1613 | MZUSP PL 1008 | KC608261 | - | KC608493 | KC608376 | KC614491 | MT468598 |
| *Cratera piguaiaboja* sp. nov. | P.N. Bocaina / SP | F2828 | MZUSP PL 458 | MT437773* | - | MT441693* | MT441716* | MT468585* | - |
| *Cratera piguaiaboja* sp. nov. | P.N. Bocaina / SP | F2829 | MZUSP PL 459 | MT437774* | - | MT441694* | MT441717* | MT468586* | - |
| *Cratera piguaiassu* sp. nov. | P.N. Bocaina / SP | F2025 | MZUSP PL 2146 | MT437763* | - | MT441685* | MT441708* | MT468577* | MT468599 |
| | | F2807 | MZUSP PL 1050 | KC608284 | - | KC608516 | KC608399 | KC614510 | MT468609 |
| | | F2821 | MZUSP PL 1052 | KC608287 | - | KC608519 | KC608402 | KC614513 | MT468611 |
| | | F2825 | MZUSP PL 2150 | MT437772* | MT468631* | MT441692* | MT441715* | MT468584* | MT468612 |
| | | F2834 | MZUSP PL 2151 | MT437775* | MT468632* | MT441695* | MT441718* | MT468587* | MT468613 |
| *Cratera piguaiatui* sp. nov. | P.N. Bocaina / SP | F2031 | MZUSP PL 1014 | KC608268[c] | MT468625* | KC608500 | KC608383 | KC614497 | MT468600 |
| | | F2040 | MZUSP PL 2147 | MT437764*[c] | - | MT441686* | MT441709 * | MT468578* | MT468601 |
| | | F2054 | MZUSP PL 2148 | MT437765* | - | MT441687* | MT441710 * | MT468579* | MT468602 |
| | | F2798 | MZUSP PL 2149 | MT437770*[c] | - | MT441691* | MT441714* | MT468583* | MT468608 |
| | | F2809 | MZUSP PL 1051 | MT437771*[c] | MT468630* | KC608517 | KC608400 | KC614511 | MT468610 |
| | P.N. Itatiaia / RJ | F5178 | MZUSP PL 2154 | MT437781* | MT468633* | MT441696* | MT441719* | MT468588* | MT468617 |
| *Cratera pseudovaginuloides* | P.N. Órgaõs / RJ | F1244 | MZUSP PL 670 | KC608251 | MT468622* | KC608483 | KC608366 | KC614482 | MT468593 |
| | | F1245 | MZUSP PL 671 | KC608252 | - | KC608484 | KC608367 | KC614483 | MT468594 |
| *Cratera tamoia* | P.N. Órgaõs / RJ | F1139 | MZUSP PL 665 | KC608246 | MT468621* | KC608478 | KC608361 | KC614478 | MT468592 |
| | | F1336 | MZUSP PL 672 | KC608254 | MT468623* | KC608486 | KC608369 | KC614484 | MT468595 |
| **Outgroup** | | | | | | | | | |

| | | | | | | | | | |
|---|---|---|---|---|---|---|---|---|---|
| *Obama anthropophila* | P.N. Itajaí / SC | F1399 | MZUSP PL 1007 | KC608256 | MT468624* | KC608488 | KC608371 | KC614486 | MT468596 |
| *Obama ladislavii* | | F1418 | MZUSP PL 681 | KC608258 | - | KC608490 | KC608373 | KC614488 | MT468597 |
| *Obama josefi* | FLONA[b] | F3403 | MZUSP PL 1075 | KC608318 | - | KC608552 | KC608435 | KC614538 | MT468614 |

2    [a] Vouchers are deposited in the Museu de Zoologia da Universidade de São Paulo (MZUSP)

3    [b] Floresta Nacional de São Francisco de Paula

4    [c] Short fragment

5    *This study